

The Mid-Infrared Colours of Galactic Bulge, Disk and Magellanic Planetary Nebulae

J.P. Phillips¹ and G. Ramos-Larios^{1,2}

¹ Instituto de Astronomía y Meteorología, Av. Vallarta
No. 2602, Col. Arcos Vallarta, C.P. 44130 Guadalajara,
Jalisco, México e-mail : jpp@astro.iam.udg.mx

Current address:

² Instituto de Astrofísica de Andalucía, IAA-CSIC
C/ Camino Bajo de Huétor # 50, 18008,
Granada, Spain e-mail : gerardo@iaa.es

Abstract

We present mid-infrared (MIR) photometry for 367 Galactic disk, bulge and Large Magellanic Cloud (LMC) planetary nebulae, determined using GLIMPSE II and SAGE data acquired using the Spitzer Space Telescope. This has permitted us to make a comparison between the luminosity functions of bulge and LMC planetary nebulae, and between the MIR colours of all three categories of source. It is determined that whilst the 3.6 μm luminosity function of the LMC and bulge sources are likely to be closely similar, the [3.6]-[5.8] and [5.8]-[8-0] indices of LMC nebulae are different from those of their disk and bulge counterparts. This may arise because of enhanced 6.2 μm PAH emission within the LMC sources, and/or as a result of differences between the spectra of LMC PNe and those of their Galactic counterparts. We also determine that the more evolved disk sources listed in the MASH catalogues of Parker et al. and Miszalski et al. (2008) have similar colours to those of the less evolved (and higher surface brightness) sources in the catalogue of Acker et al. (1992); a result which appears at variance with previous studies of these sources.

Key Words: planetary nebulae: general --- infrared: ISM

1. Introduction

The MIR fluxes of planetary nebulae (PNe) depend upon a broad range of emission mechanisms, including warm dust continuum emission, emission associated with PAH bands and plateau features, ionic and atomic permitted and forbidden line transitions, the quadrupole transitions of H₂, and the underlying free-free and bound-free components of gaseous continuum emission. Given that at least certain of these components depend upon the degree of excitation of the gas, the mass and evolutionary status of the shells, the presence or otherwise of shock and fluorescent excitation, and the chemical composition of the progenitors, it follows that MIR spectra may vary appreciably between differing nebular outflows.

In particular, we note that the abundances of Galactic bulge PNe (GBPNe) differ from those of Galactic disk sources (GDPNe), tending as they do to have slightly higher metallicities (e.g. Wang & Liu 2007; Maciel et al. 2006; Gorny et al. 2004; although see also Exter et al. (2004) and Casassus et al. (2001), where it is noted that O/H ratios are indistinguishable within rather large error limits), lower C/O ratios (Wang & Liu 2007; Casassus et al. 2001), and differing abundance trends for other elements indicative of markedly different evolutionary histories (see e.g. Cuisinier et al. 2002). It has also been noted that the sources are likely to possess differing radial trends in abundance gradient; that bulge sources have a larger incidence of oxygen rich features, such as the crystalline silicate bands at $\sim 26\text{-}36\ \mu\text{m}$ (Perea-Calderón et al. 2009; Gutenkunst et al. 2008; Casassus et al. 2001); and that a larger fraction of bulge sources sport both oxygen and carbon rich features in the MIR (Gutenkunst et al. 2008). Indeed, such mixed features appear to be present in all of the 26 sources investigated by Perea-Calderón et al. (2009).

The GDPNe are noted for radial gradients in abundance, with those located close to the Galactic centre having higher metallicities (see e.g. Martins & Viegas (2000); Maciel & Quireza (1999), Maciel & Koppen (1994); Pasquali & Perinotto (1993); Amnuel (1993); Samland et al. (1992); Koppen et al. (1991); and Faundez-Abans & Maciel (1986)). This is attributed to the synthesis of elements over the lifetime of the Galaxy, and the varying degrees to which they enrich the interstellar medium, and affect the abundances of the progenitors.

Finally, and at the other extreme, it has been noted that PNe within the Magellanic Clouds have metallicities which are between ~ 0.25 dex (LMC) and ~ 0.5 dex (SMC) lower than those of GDPNe (Maciel et al. 2006, 2008; Chiappini et al. 2008); a disparity which may lead to differences in ionising fluxes, central star luminosities, emission line strengths, and grain formation and emission characteristics.

It is therefore of interest to explore such influences upon the MIR characteristics of the nebulae, a program which may be undertaken through either spectroscopy [see e.g. Gutenkunst et al. (2008) and Perea-Calderón (2009) for bulge nebulae, Bernard-Salas et al. (2005) and Stanghellini et al. (2007) for LMC and SMC PNe, and Hora et al. (2004) and Phillips & Ramos Larios (2008a) for GDPNe] or broad-band photometry and mapping [see e.g. Hora et al. (2008) for LMC sources, and Phillips & Ramos-Larios (2008a, b); Ramos-Larios & Phillips (2008a, b); Hora et al. (2004); Cohen et al. (2007a); Su et al. (2004, 2007); and Ueta (2006) for GDPNe].

We shall, in the following, be adding to these latter data bases, and investigating the MIR colours of GBPNe contained within the catalogue of Van de Steene & Jacoby (2001); of LMC nebulae in the catalogue of Reid & Parker (2006); and of disk PNe listed in the catalogues of Acker et al. (1992), Parker et al. (2006; MASH I) and Miszalski et al. (2008; MASH II). These latter catalogues refer to nebulae having a large range of evolutionary states, from the predominantly less evolved and higher surface brightness sources of Acker et al. (1992), to the larger, more evolved, and predominantly lower surface brightness nebulae of the two MASH catalogues.

We shall compare the colours and magnitudes of these disparate groups of nebulae, and note a broad range of similarities and a variety of differences. We shall also note a difference between the characteristics of our present MASH nebulae, and the results of previous analyses of these sources.

2. The Observational Data Base

We have acquired photometry and mapping of a wide range of Galactic disk, Galactic bulge, and LMC planetary nebulae using data deriving

from the second Galactic Legacy Infrared Midplane Survey Extraordinaire (GLIMPSE II) (Benjamin et al. 2003), and the program Surveying the Agents of a Galaxy's Evolution (SAGE; Meixner et al. 2006). Both of these surveys were undertaken using the Spitzer Space Telescope (SST; Werner et al. 2004). Details of the instrumentation and data processing for these programs have been described in previous publications (see e.g. Hora et al. 2004, 2008; Phillips et al. 2008a, b), and we shall note only the most salient features of importance to this analysis.

The catalogues and mosaics of the GLIMPSE II project were published over a period extending between 2007 and the Spring of 2008, and cover approximately 25 square degrees of the Galactic plane within the regimes $350^\circ < l < 10^\circ$, and $-2^\circ < b < +2^\circ$. The mapping was undertaken using the Infrared Array Camera (IRAC; Fazio et al. 2004), and employed filters having isophotal wavelengths (and bandwidths $\Delta\lambda$) of $3.550 \mu\text{m}$ ($\Delta\lambda = 0.75 \mu\text{m}$), $4.493 \mu\text{m}$ ($\Delta\lambda = 1.9015 \mu\text{m}$), $5.731 \mu\text{m}$ ($\Delta\lambda = 1.425 \mu\text{m}$) and $7.872 \mu\text{m}$ ($\Delta\lambda = 2.905 \mu\text{m}$). The spatial resolution varied between ~ 1.7 and ~ 2 arcsec (Fazio et al. 2004), and is reasonably similar in all of the bands, although there is a stronger diffraction halo at $8 \mu\text{m}$ than in the other IRAC bands. This leads to differences between the point source functions (PSFs) at ~ 0.1 peak flux. The maps were published at a resolution of 0.6 arcsec/pixel.

Further details of the GLIMPSE data processing are provided in http://www.astro.wisc.edu/sirtf/glimpse1_dataproduct_v2.0.pdf.

We have used these recent GLIMPSE II results to undertake photometry and mapping of PNe close to the projected location of the Galactic centre. The positional listing of the nebulae derives from four principal catalogues. In the first place, the Acker et al. (1992) catalogue of Galactic PNe contains all of the sources identified prior to 1992. Most of these have reasonably high surface brightnesses, and correspond to less evolved nebular outflows, although there is also a sprinkling of larger, fainter, and (usually) higher Galactic latitude sources which correspond to later phases of nebular evolution. The fraction of the latter, more evolved sources is relatively small, however, and is expected to be even smaller within our present Galactic centre sample.

More recently, this list has also been supplemented by the so-called MASH I and MASH II catalogues of Parker et al. (2006) and Miszalski et al. (2008). These sources were detected as a result of investigation of the Anglo-Australian Observatory UK Schmidt Telescope (AAO/UKST) $H\alpha$ survey of the southern Galactic plane (Parker et al. 2005), and represent outflows which are mostly larger, fainter, and correspond to more evolved nebular shells.

Insofar as we can make a judgement based upon $H\beta$ or radio fluxes, and the angular sizes of the nebular shells, it appears that few if any of the present MASH and Acker et al. sources correspond to GBPNe. We shall be assuming that the large majority of these nebulae correspond to foreground disk PNe – many possibly located in the inner Galactic disk, where metallicities are higher.

The fluxes of the sources have been measured using a variety of circular or elliptical apertures, and employing GLIMPSE II FITS pipeline images. Backgrounds were estimated for nearby regions of sky, and using the same aperture sizes and shapes as were used to determine the total nebular fluxes. These were then subtracted from the nebular results, and the fluxes converted to magnitudes using the Vega calibration of Reach et al. (2005).

Whilst such results are entirely reasonable where source sizes are small (< 8 - 9 arcsec), scattering of light in the array focal plane affects larger aperture measurements – an effect which is particularly important at $5.0\ \mu\text{m}$ and $8.0\ \mu\text{m}$, and may arise due to scattering in an epoxy layer between the detector and multiplexer (Cohen et al. 2007b). It is therefore necessary to modify fluxes as described in Table 5.7 of the SST IRAC handbook (see e.g. http://ssc.spitzer.caltech.edu/irac/dh/iracdatahandbook_3.0.pdf), and this leads to corrections of maximum order 0.944 at $3.6\ \mu\text{m}$, 0.937 at $4.5\ \mu\text{m}$, 0.772 at $5.8\ \mu\text{m}$ and 0.737 at $8.0\ \mu\text{m}$. We have applied these changes for the larger sources considered here. However, the precise values of these corrections also depend on the underlying surface brightness distribution of the source, and for objects with size \sim several arcminutes it is counselled to use corrections which are somewhat smaller (i.e. between the values cited above and unity). The handbook concludes that “this remains one of the largest outstanding calibration problems of IRAC”.

It is therefore possible that some of the photometry for the larger sources may have been over-corrected, although errors are unlikely to exceed a tenth of a magnitude or so – and are certainly insufficient to radically affect the analysis below.

Finally, errors in these fluxes tend to be dominated by uncertainties in sky and nebular subtraction. In particular, sky background fluxes may be afflicted by weak stellar emission, sometimes barely discernable in images of the fields; variable levels of diffuse Galactic emission (particularly important at wavelengths $\geq 8 \mu\text{m}$); and components arising from photon and instrumental noise. We have determined these contributions in assessing the errors quoted in Tables 1 & 2, estimating the most important of these (background subtraction) by measuring the sky at a variety of locations about the sources.

The corresponding photometry for 26 Acker et al. (1992), and 20 MASH I & II sources are listed in Table 1, where we specify the Galactic coordinates of the sources (column 1), the source catalogue (column 2); the name of the source (column 3), and 3.6 μm to 8.0 μm photometry and associated errors (columns 4 to 11).

Some of the first identifications of Galactic Bulge PNe were undertaken by Pottasch & Acker (1989), selected on the basis of their proximity to the Galactic centre, small angular dimensions and low H β flux levels. Subsequent listings of these sources have been provided by Beaulieu et al. (1990) and Van de Steene & Jacoby (2001), whilst a catalogue of a further 400 sources has been described by Acker et al. (2006). Most of these listings are either unavailable at present (viz. the case of the Acker et al. catalogue), or refer to nebulae which are, for the most part, located outside of the limits of the GLIMPSE II survey. An exception in this respect is the survey of Van de Steene & Jacoby (2001), in which the authors identified 64 sources in the radio continuum at 3 and 6 cm. We have determined IRAC photometry for approximately half of these sources, using data deriving from the GLIMPSE II PSC. For the remaining cases, we have determined MIR photometry from GLIMPSE imaging results, and using the procedures described above; a strategy which is necessary where the sources are appreciably extended, or have fluxes falling below the inclusion limits of the PSC. Photometry for these sources is listed in Table 2, where the sequencing of the columns is similar to that in Table 1.

Finally, Hora et al. (2008) have published equivalent photometry for nebulae within the LMC, making use of data products deriving from the Spitzer SAGE program (Meixner et al. 2006). In this case, the IRAC instrument, and the Multiband Imaging Photometer for Spitzer (MIPS; Reike et al. 2004) were used to perform an unbiased $\sim 7^\circ \times 7^\circ$ survey centred on the LMC. The catalogue of Hora et al. contains some 275 sources, and makes use of the listing provided by Leisy et al. (1997). Reid & Parker (2006) have subsequently published positions for a further 460 new possible, likely or true PNe, however, and we have determined Spitzer and 2MASS magnitudes for these sources using the SAGE PSC. This catalogue, corresponding to the version published in Winter of 2008, is described as being “more reliable” than previous versions of the document; it includes sources having a S/N > 10 at $8 \mu\text{m}$, and > 6 in the other wavebands, and excludes near-neighbour detections within a radius of 2 arcsec of the sources. It is clear however that not all of the gremlins have been successfully removed, and there is some duplication of photometry for certain of the sources.

We have identified MIR sources within 3 arcsec of the positions listed by Reid & Parker (2006), and assumed that the PNe correspond to the MIR detections with smallest positional offsets. The mean positional displacement is found to be 1.0 arcsec.

Details of the photometry are listed in Table 3, with the first column giving the number of the source in the catalogue of Reid & Parker, followed by the Galactic position (columns 2 and 3), the name and status of the source (columns 4 & 5; where T \equiv True, P \equiv Possible, and L \equiv Likely), and photometry and associated errors (columns 6-19). The final column gives the displacement between the SAGE source position and the catalogue coordinates of Reid & Parker (2006).

We shall, for the purposes of the following analysis, fold this photometry in with the results of Hora et al. (2008), yielding a sample of some 178 nebulae for which photometry is available in all four of the IRAC bands. These results will subsequently be analysed within colour-colour and colour-magnitude planes, as described in Sects. 3 & 4.

3. The MIR Colour-Magnitude Diagrams

Hora et al. (2008) have undertaken an MIR colour-magnitude analysis for PNe located in the LMC and Galactic disk, taking account of the differing distance moduli of the respective groups of sources. Although such an analysis is certainly of interest, and leads to some intriguing results, it relies upon the extremely uncertain distances to the GDPNe. It would be more useful, under these circumstances, to compare the relative distributions of sources for which distances to the nebulae are reasonably well established.

We have undertaken such an analysis in Figs. 1 and 2, where we compare the distribution of LMC PNe (indicated by the smaller blue disks) with those of the GBPNe (larger red disks). In this case, the magnitudes of the LMC nebulae have been modified so as to correspond to the values they would have at the Galactic centre; where the distance to the LMC is assumed to be 48.1 kpc (Macri et al. 2006), and that of the Galactic centre is 7.62 ± 0.32 kpc (Eisenhauer et al. 2005). Subsequent to undertaking this analysis, we noted the publication, by the same team of authors, of an upgraded distance 8.33 ± 0.35 kpc (Gillissen et al. 2008), suggesting that the distance to the centre is still very much a work in progress. This difference in distances may imply the need for a further correction of ~ 0.2 mag when comparing LMC and bulge PNe luminosities.

Finally, we have also shown the completeness limits of the SAGE survey at 3.6 and 8.0 μm , below which source detection efficiencies are appreciably reduced. The values for these limits are taken from the SAGE delivery document at http://irsa.ipac.caltech.edu/data/SPITZER/SAGE/doc/SAGEDataDescription_Delivery2.pdf, and are important in defining the apparent distribution of LMC PNe.

Several differences may be noted between the distributions of bulge and LMC sources. It is clear for instance that the GBPNe lie predominantly in the range $[3.6] > 9$ mag and $[3.6]-[8.0] < 3$ – a regime which is below the 8 μm completeness limit of the LMC PNe. It is therefore apparent that if the $[3.6]$ luminosity functions of the populations are in any way comparable, then we are failing to measure a very large fraction of the Magellanic PNe.

Note in this respect that differences of extinction are unlikely to affect this comparison between the sources. Even where there is a difference of $\Delta A_V = 10$ mag between the extinctions of the bulge and LMC sources, for instance, the relative shifts of the populations would be reasonably modest (see the corresponding reddening vector in Fig. 1) We shall later provide evidence that differences in extinction may in fact be very much less (see Sect. 5). Similarly, although some of the scatter along the vertical axis may arise from differences in line-of-sight distance, this is unlikely to be greater than $\Delta[3.6] \sim 0.35$ mag, and will be comparable for both of the populations.

Despite the fact that the LMC sample is far from complete, and the GBPNe may be magnitude limited because of corresponding radio detection limits, it is clear that the $3.6 \mu\text{m}$ luminosity functions of the bulge and Magellanic sources are very closely comparable, and peak close to $[3.6] = 12.5$ mag (Fig. 3). The somewhat slower fall-off of LMC sources to lower $3.6 \mu\text{m}$ luminosities (i.e. higher magnitudes $[3.6]$) may be attributable to the incompleteness of the sample having $[3.6] > 12$ mag – and the corresponding reduction that this causes in peak source fractions.

It may finally be noted that although the range in $[3.6]$ magnitudes is of order ~ 5 mag for the GBPNe, there appears to be little correlation between the $3.6 \mu\text{m}$ magnitude on the one hand, and the $[3.6]$ - $[8.0]$ index on the other. The levels of dispersion, and mean value of $[3.6]$ appear to be reasonably invariant and independent of the colour.

Somewhat similar results apply for the LMC sources as well, although our analysis is compromised by the relative incompleteness of the LMC sample.

The various tendencies noted above are also apparent when one compares the $[8.0]$ and $[3.6]$ magnitudes directly, as in Fig. 4. Although the sample of bulge nebulae is comparatively small (see the upper panel), that of the LMC nebulae is very much larger (lower panel).

It is apparent, from the LMC sample, that providing that $[3.6] > 11$ and $[8.0] > 8$, then there is very little variation in $[3.6]$ - $[8.0]$ colours as a function of either of these magnitudes. Furthermore, it is clear that the $[3.6]$ - $[8.0]$ index is very tightly constrained, and takes a maximum value

close to ~ 3.8 mag. This presumably indicates the presence of an upper limit flux difference attributable to the 7.7 and 8.6 μm PAH band features.

The trend between the 4.5 and 3.6 μm magnitudes (black diamonds), by contrast, follows a linear relation about the free-free locus (indicated by the diagonal dashed line). It will be noted that there is a considerable scatter about this trend, with nebular points located along two closely parallel and overlapping lines. These two trends represent pure gaseous (upper trend), and dominant stellar emission (lower trend). The fact that the gaseous trend is ~ 0.3 mag higher than the bremsstrahlung relation presumably arises due to extra components of flux in the 4.5 photometric band, such as $\text{Br}\alpha$, $[\text{Ar VI}]$ and $[\text{Mg IV}]$, and some shift in values due to interstellar extinction.

The corresponding variation of $[3.6]-[8.0]$ colours with 8.0 μm magnitudes is illustrated in Fig. 2. Here again, the limited completeness of the 8.0 μm SAGE sample greatly constrains the distribution of LMC sources, and very few nebulae possess $[8.0] > 9.5$ mag ($\equiv [8.0] > 13.5$ mag at the distance of the LMC). This constraint upon sample sizes is more severe than was the case at 3.6 μm , and leads to a marked difference between the luminosity functions of the bulge and LMC sources (Fig. 3).

Finally, it is worth noting that the bulge sources show a systematic trend of $[3.6]-[8.0]$ colour with 8.0 μm magnitude, a variation which is particularly evident where $[3.6]-[8.0] > 3.0$.

4. The Colour-Colour Diagrams

Unlike the case of the magnitude-colour diagrams, the colour-colour diagrams enable us to make direct comparisons between all four groupings of source considered here - the LMC PNe, the GBPNe, and the MASH and Acker et al. populations of the GDPNe. Even in this case, however, some care must be taken in interpreting the results, and trends within the colour plane may be influenced by the magnitude completeness limits described above.

We shall consider the distributions of sources within the [3.6]-[4.5]/[4.5]-[8.0] (Fig. 5), and [3.6]-[4.5]/[5.8]-[8.0] and [5.8]-[8.0]/[4.5]-[5.8] planes (Fig. 6) separately below.

4.1 The [3.6]-[4.5]/[4.5]-[8.0] Colour Plane

It is clear, from Fig. 5, that all of the sources occupy a similar regime of the [3.6]-[4.5]/[4.5]-[8.0] colour plane. There are however differences, and these help in defining the emission mechanisms responsible for these trends. In the first place, although it is clear that the ranges of [3.6]-[4.5] index are similar for all classes of nebulae, there is a tendency for LMC sources to be concentrated about [3.6]-[4.5] \sim 0.8 mag. This trend is even more apparent in Fig. 7, where we compare trends for all three categories of source. The nebulae in the upper three curves correspond to sources which have been detected in all four of the IRAC bands; that is, they correspond to exactly the same sample of PNe as is represented in Fig. 5. It is apparent, for these cases, that whilst the LMC sources peak within a range Δ ([3.6]-[4.5]) \sim 0.6 mag, the distributions for GDPNe and GBPNe are very much broader.

Some clue as to what might be happening may be determined when one plots the distribution of LMC sources having *no* 5.8 or 8.0 μ m emission, as is the case for the lowermost curve of Fig. 7. In this case, the sources are again located within a narrow range of colours, but peak at indices close to [3.6]-[4.5] \sim 0.1 mag. There are several possible explanations for these trends.

In the first place, we note that nearly half of the Spitzer PNe appear to have no MIR dust emission at all (see e.g. Stanghellini et al. 2007); in which case 5.8 and 8.0 μ m fluxes may fall below levels of Spitzer detectability. Such nebulae are also likely to have [3.6]-[4.5] indices which are quite distinct from those of their more dusty counterparts – and perhaps similar to what has been noted in our analysis above.

Models of radiatively accelerated AGB mass loss also suggest that low dust-producing progenitors may also have lower rates of mass-loss (see e.g. Winters et al. 2000; Sedlmayr & Dominik 1995); a situation which may result in lower levels of shorter-wave bremsstrahlung emission, and a dominance by the stellar continua.

Finally, we note that low [3.6]-[4.5] indices may also ensue where shell and progenitor masses are intrinsically smaller, and/or where the nebulae are highly evolved, shell surface brightness are small, and the nebulae fall, yet again, below levels of instrumental detectability (see our further discussion in Sect. 7).

By contrast, the source completeness limits for the bulge and disk sources are very much less severe, and the upper two curves of Fig. 7 contain both categories of source – nebulae in which shell emission is weak, and central star continua are relatively strong, and where the reverse is the case, and fluxes are dominated by shell components of emission alone. This leads to the prominent double-peaked profile for the bulge sources, and the comparatively broad distribution of sources noted for disk PNe.

Having said this, Hora et al. (2008) have noted that sources having large values of [4.5]-[8.0] also tend to have somewhat smaller indices [3.6]-[4.5] – a feature which is apparent in Fig. 5 where [4.5]-[8.0] > 3. They suggest that this may arise because of strong 3.3 μm PAH band emission, and/or the contribution of the $\text{P}\gamma$ transition at 3.74 μm , both of which are located within the 3.6 μm channel. Where this is the case, then it is apparent that it may contribute to sources having intermediate values of [3.6]-[4.5] (although the influence of $\text{P}\gamma$ is likely to be small, not least because increases in the strength of this particular transition will be more than offset by the contribution of $\text{Br}\alpha$ in the 4.5 μm band).

The distributions of sources with respect to the [4.5]-[8.0] colour axis, by contrast, appear to be much more similar – all classes of nebulae have similarly broad ranges of scatter. Here again, however, whilst the trends in source fraction (illustrated in Fig. 8) confirm that this is the case, there are also far from negligible differences. The LMC sources tend to be weighted towards larger values of the index, the bulge sources more inclined towards lower indices, and the GDPNe extend over the full range of indices, from the very small (~ 0.1) to the very large (~ 5).

These differences can, yet again, be partially attributed to the detection limits of the Spitzer SAGE survey. Given that we are including only those nebulae in which all four bands have been detected, it is

apparent that LMC sources having lower 5.8 and/or 8.0 μm shell emission fall outside of the sample illustrated in Fig. 8. The excluded sources are likely to include a large fraction of nebulae in which central star continua are appreciable, and [4.5]-[8.0] colours are reduced.

4.2 The [3.6]-[4.5]/[5.8]-[8.0] and [5.8]-[8.0]/[4.5]-[8.0] Colour Trends

The final two colour diagrams are illustrated in Fig. 6, and show the most radical differences in colour between the nebulae considered here. Considering firstly the [3.6]-[4.5]/[5.8]-[8.0] distribution, it is apparent that whilst the bulge and disk nebulae extend over a range $-0.2 < [5.8]-[8.0] < 4$, with a few outliers extending as high as $[5.8]-[8.0] \sim 5$, the LMC nebulae are strongly truncated to the range $[5.8]-[8.0] < 2$. This is even more clearly apparent in Fig. 8, where it is seen that the peak in LMC sources is narrow, and centred close to $[5.8]-[8.0] \sim 1.75$. There are at least three possible reasons for this disparity in colours. In the first place, a large fraction of LMC nebulae appear to possess no MIR dust emission at all. This is likely to introduce variations in colours similar to those noted above (see Sect. 6).

Most of the LMC nebulae appear to possess spectra dominated by carbon-rich dust emission features, however (Stanghellini et al. 2007). For these cases, it may be that 7.7 and 8.6 μm PAH features within the 8.0 μm band are very much weaker than the 6.2 μm feature within the 5.8 μm band. This may also be allied to weaker dust continuum emission with the 8.0 μm band.

Alternatively, it is possible that PAH emission within the 5.8 μm band is relatively stronger, and uniquely responsible for the reduction in [5.8]-[8.0] indices.

There is in fact some further evidence that this latter mechanism may be responsible for explaining these disparities. When one compares the [5.8]-[8.0] and [4.5]-[5.8] colours, as in the lower panel of Fig. 6, then it is apparent that whilst the [5.8]-[8.0] indices are much reduced within the LMC nebulae, the [4.5]-[5.8] indices are significantly higher. This suggests that it is the [5.8] magnitudes which may be appreciably truncated.

Finally, it is worth noting that the range of [4.5]-[8.0] indices is similar in all categories of source (see Figs. 5 & 8). Given that there is no PAH emission within the 4.5 μm photometric band, this suggests that levels of 7.7 and 8.6 μm PAH emission are at least comparable, if not necessarily the same.

It is therefore possible that the strength of the 6.2 μm PAH and plateau features are relatively larger in LMC nebulae as compared to their strengths in the Galactic bulge and disk PNe.

We shall discuss these trends further in Sect. 7, where it will be pointed out that a variety of mechanisms may be responsible for modifying the PAH emission band strengths.

A final interesting aspect of the distribution in Fig. 6 relates to the Galactic disk components themselves. It will be noted that the Acker et al. (1992) disk sources, represented by the black diamonds, have a distribution which is not very much different from that of their MASH counterparts (represented by the squares). This result differs from that noted in previous studies of these nebulae (Cohen et al. 2007a), where it was determined that the colour range of MASH PNe was very much smaller than those of the Acker et al. sources.

5. Near-infrared Colour distribution

The distribution of 2MASS indices for bulge and LMC PNe is illustrated in Fig. 9, wherein we also indicate the trends observed for GDPNe (Ramos-Larios & Phillips 2005). The indices include all of the sources, irrespective of whether they were detected in longer wavelength Spitzer photometry or not, and are located within a couple of arcsecs of the specified PNe positions.

It can be seen that whilst a reasonable fraction of the colours appear to correspond to heavily reddened PNe bremsstrahlung emitting shells (most of those having $H-K_S > 0.65$ mag), the larger part of the LMC detections appear to concentrate close to $J-H \sim 0.5$ mag, $H-K_S \sim 0.15$ mag, or along a diagonal line to the upper right-hand side of this grouping. If our identifications are correct, it would therefore seem likely that most of these sources have fluxes dominated by the central star continua, and are experiencing varying levels of interstellar

reddening. Where this is the case, and one employs the extinction coefficients of Gordon et al. (2003), then this would give LMC extinctions of ≈ 7 mag or so.

The bulge nebulae, on the other hand, tend to be congregated close to $J-H \sim 1.25$ mag, $H-K_S \sim 0.54$ mag – a situation that can again be interpreted in terms of stellar dominated continua, and high levels of extinction. Where this is the case, and assuming that reddening can be approximated by the prescription of Cardelli et al. (1989) for $R_V = A_V/E_{B-V} = 3.1$, then this implies that extinction for the main body of the sources is of order $A_V = 11.6$ mag. The differential extinction between these groups of nebulae, the LMC sources on the one hand and the GBPNe on the other, would then appear to be of order $\Delta A_V \sim 4.6$ mag. However, it should be noted that there is evidence that values of R_V towards the Galactic centre may be much less than supposed above, with Walton et al. (1993) finding $R_V = 2.3$, and Ruffle et al. (2004) determining $R_V = 2.0$. If this latter value is adopted, then mean values of A_V would climb to ~ 15 mag or so.

All of these estimates of extinction seem to be somewhat on the large side, however. For instance, the bulge sources of Gutenkunst et al. appear to have typical extinctions of close to $C \sim 2$, which would imply $A_V \sim 4.25$ mag for $R_V = 3.1$. Similarly, we note that LMC planetaries seem to have typical extinctions $\langle E_{B-V} \rangle \cong 0.13$ mag (Villaver et al. 2003, 2004), which might imply values $A_V \cong 0.44$ where one uses $R_V = 3.41$ (Gordon et al. 2003). So on this basis, and with these lower extinctions, it is clear that the difference in extinction would be of order $A_V(\text{GBPNe}) - A_V(\text{LMC}) \sim 3.8$ mag, and somewhat larger than this if the lower values of R_V for the Galactic bulge are employed.

So it seems that whatever way one spins the coin, the mean difference in extinction between bulge and LMC PNe is likely to be ~ 4 mag or so. However, the difference in the absolute values of these extinctions is certainly troubling, and brings into question whether the supposedly stellar dominated sources might not contain appreciable levels of plasma emission, or whether some of these apparent identifications refer to differing sources altogether; perhaps later G-M stars in the line-of-sight. It follows that the present 2MASS results, and the corresponding NIR photometry of Hora et al. (2008) should be treated with a certain degree of caution.

6. Discussion

It is clear, from Sects. 4 & 6, that we are observing a broad range of shell emission mechanisms within the MIR; processes which result in bremsstrahlung emission, central star continuum emission (both of the latter particularly strong at 3.6 and 4.5 μm), permitted and forbidden line emission, and (most probably) various shocked and/or fluorescently excited transitions of H_2 . The dominant components at longer wavelengths, however, are likely to be the PAH band features, gaseous thermal continuum emission, and underlying smooth components of continuum arising from amorphous carbon or silicate grains. Given that many of the latter particles are located within PDRs, and that the PDRs may extend a considerable distance from the central ionised zones, then this may explain the broad increases in source size observed at longer IRAC wavelengths, detected both in the present nebulae (Phillips & Ramos-Larios 2009, in preparation) and in other PNe (see e.g. Phillips & Ramos-Larios 2008a, b).

Such mechanisms also go a long way to explaining the large ranges of colour index noted in Figs. 5-6. Generally speaking, whilst dust continuum and PAH emission will tend to shift PNe towards larger values of [4.5]-[8.0], H_2 and ionized gas emission will tend to force sources in a reverse direction. Similarly, whilst PAH and ionized gas emission tends to reduce indices [3.6]-[4.5], dust continuum emission would tend to lead to a reverse effect.

Given that various of these mechanisms are compositionally dependent, then it might be anticipated that the distributions of colours might also vary between the groups of sources considered here. Thus for instance, it is well established that PN abundances in the Magellanic Clouds follow the trends detected for a variety of other sources, including stars and HII regions, and imply abundances which are significantly less than those of their Galactic counterparts. Such differences in abundance are also likely to be reflected in the peculiarities of their MIR spectra, noted for instance in the Spitzer analysis of Stanghellini et al. (2007). It appears from this that nearly half of their sources show no MIR dust emission at all, and that MIR indices are likely to be dominated by gas thermal continua and line contributions. Where dust band emission is detected, then it appears

that most of the sources contain SiC or PAH emission components; the incidence of silicate features is relatively small.

Similarly, whilst the metallicities of GBPNe are somewhat larger than those for GDPNe, it appears that carbon abundances may be somewhat less (Wang & Liu 2007; Casassus et al. 2001). This may contribute to the larger incidence of silicate features in the MIR spectra of these sources – indeed, they are present in all of the GBPNe which have been analysed so far (Gutenkunst et al. 2008; Perea-Calderón et al. 2009).

Having said this, however, it is apparent that the bulge sources contain a larger proportion of nebulae in which carbon-rich features (e.g. the SiC band at 10.5-12.7 mm; see e.g. Forrest et al. 1975; Anderson et al. 1999; Casassus et al. 2001) and oxygen-rich features (such as the crystalline silicate features at 26-37 μm ; see e.g. Molster et al. 2002) are observed within the self-same shells (Gutenkunst et al. 2008; Perea-Calderón et al. 2009) – a trend which appears to be much more common than is the case for GDPNe. This may arise because the incidence of binary induced morphologies is larger in the bulge (viz. Zijlstra 2007), and as a result of the tendency for many bipolar sources to have inner C-rich bipolar outflows, surrounded by outer O-rich tori (see e.g. the discussion of Gutenkunst et al. 2008). The crystalline silicate features may arise where AGB winds impact these tori and anneal the dust (Edgar et al. 2008). It has also been suggested that late thermal pulses at the end of the AGB phase may lead to changes in C/O ratios within the flows (Waters et al. 1998); that evaporation of Oort-belt comets may release crystalline silicates (Cohen et al. 1999); and that various other processes involving binary systems, variations in hot-bottom burning, and brown dwarfs or planets may also explain these trends (see the slightly more detailed discussions of Gutenkunst et al. (2008) and Perea-Calderón et al. (2009), and references therein). It is therefore clear that there is no shortage of explanations, but still as yet little understanding of these trends.

So, there is considerable evidence for compositional differences between GDPNe, GBPNe and LMC PNe, and the question arises as to whether such variations are also reflected in the colour-colour diagrams described in Sect. 4.

We have already pointed out that there appear to be marked differences in distribution with respect to the [3.6]-[4.5] and [4.5]-[8.0] indices (see Figs. 5-8). The LMC sources tend to be more narrowly peaked, and located towards higher values of these indices, for instance. It was pointed out however that such trends may occur where one is excluding shells in which MIR dust emission is reduced, and 5.8 μm and/or 8.0 μm intensities are small; a result which applies to nearly half of the LMC nebulae investigated by Stanghellini et al. (2007). This results in the elimination of sources in which stellar continua may be important, and/or possess 3.6 and 4.5 μm fluxes which are affected by a differing balance of emission mechanisms (e.g. reduced bremsstrahlung and/or 3.2 μm PAH emission), leading to [3.6]-[4.5] and [4.5]-[8.0] indices which are correspondingly reduced.

A similar analysis for more evolved sources suggests that comparable trends would apply for these sources as well. As nebulae evolve towards their turn-over points in the HR plane, where hydrogen burning ceases, then central star temperatures increase (e.g. Vassiliadis & Wood 1994)) and absolute magnitudes M become larger (i.e. MIR and visual fluxes decrease; e.g. Schonberner 1981), even though bolometric luminosities remain more-or-less the same. Beyond this stage, however, the central star luminosities and temperatures go into a sharp decline, stellar absolute magnitudes remain more-or-less invariant, and shell surface brightnesses decline as $\propto R^{-5}$ (where R is the radius of the nebula). The surface brightnesses of the shells are therefore expected to decline very rapidly indeed, and will eventually fall below levels of instrumental detectability. The stellar MIR fluxes, by contrast, would remain more-or-less invariant, and eventually dominate fluxes in the shorter wave IRAC passbands.

It therefore follows that the exclusion of intrinsically fainter (or lower surface brightness) nebulae removes sources which would normally occupy lower ranges of the [3.6]-[4.5] and [4.5]-[8.0] colour regimes.

Having stated all of this, however, and taken note of other observationally driven biases as well, it is nevertheless apparent that there are intrinsic similarities and differences between the various nebular groupings. On the one hand, it is clear that despite the partial sampling of LMC nebulae, the 3.6 μm luminosity function for these sources is similar to that of the GBPNe. Similarly, it is noted that the

LMC PNe, GBPNe and GDPNe extend over similar ranges of index [4.5]-[8.0] – although there appear to be proportionately more GDPNe at the very highest values of this index (> 4).

Perhaps the sharpest disparities, however, are those noted in the [5.8]-[8.0] and [4.5]-[5.8] colours. There are at least two possibilities for explaining these results. In the first place, and as noted above, nearly half of the LMC spectra of Stanghellini et al. (2007) appear to contain no MIR dust emission at all – a complete contrast to what has so far been observed for Galactic bulge and disk PNe. So for these sources, at least, it is clear that emission would be dominated by bremsstrahlung continuum and forbidden line emission, including the strong transitions of [ArII] 6.99 μm , [ArV] 7.90 μm and [ArIII] 8.99 μm . Permitted transitions of H I, and various transitions due to H₂ may also contribute to the mix. The net result would be for limits upon the [5.8]-[8.0] and [4.5]-[5.8] indices which are consistent with those noted in Fig. 6. However, this situation is likely to apply to less than half of the LMC sources considered here, whilst many of them are likely to have 5.8 and 8 μm fluxes which exclude from the colour-colour analysis described above (i.e. causes them to fall below the Spitzer SAGE detection limits). The question then arises as to how one might explain the carbon dominated spectra of most of the other PNe – that is, those spectra in which PAH features dominate our present IRAC fluxes.

To understand what might be happening in the latter case, we note first that emission at 4.5 μm is likely to be influenced by various atomic and ionic transitions (such as Br α , the forbidden lines [Ar VI] and [Mg IV] close to 4.53 μm , and the shock or fluorescently excited $v=0-0$ S(8) and S(9) lines of H₂ at $\lambda\lambda$ 4.69 and 5.05 μm), as well as by free-free and bound-free plasma emission. There are however no PAH band features, such as are observed in the other IRAC passbands. It therefore follows that the [5.8]-[8.0] and [4.5]-[5.8] indices are likely telling us something about the relative strengths of the 6.2 PAH feature in the 5.8 μm band, and the 7.7 and 8.6 μm features in the 8.0 μm band – not to mention the related, and much broader plateau components which are associated with these contributions. It was argued, in Sect. 4.2, that the fact that the LMC sources tend to have highly restricted (and low) values of [5.8]-[8.0], larger values of [4.5]-[5.8], but rather similar indices [3.6]-[8.0], may be indicative of

enhanced 6.2 μm PAH emission – that the LMC sources have larger 6.2 μm /(7.7 μm +8.6 μm) PAH ratios than is the case for the GDPNe and GBPNe

This, should it be the case, may arise from differences in the natures and dimensions of the PAH particles, and depend upon whether they contain smaller aggregates of C atoms such as coronene, or represent larger structures such as dicoronene (see e.g. Léger & d’Hendecourt 1988). It also depends upon whether the PAH atoms are neutral or ionised.

Where ionisation is important, for instance, then this will tend to enhance C-C stretching vibrations, such as are principally responsible for the 6.2 μm PAH band feature (see e.g. Peeters et al. 2002, and the related laboratory work of Allamandola et al. 1999). The transitions responsible for the 7.7 and 8.6 μm features, by contrast, correspond to C-H in-plane bending modes (in the case of the 8.6 μm feature), and combined C-H in-plane bending and C-C stretching modes (for the remaining transitions). Ionisation of the particles may therefore shift PAH strengths in the direction noted for our LMC nebulae.

It has also been noted that small PAH grains and clusters possess differing levels of emission for the 6.2 μm feature on the one hand, and the 7.7 and 8.6 μm features on the other, with ratios $I(7.7\mu\text{m}+8.6\mu\text{m})/I(6.2\mu\text{m})$ tending to be larger in the case of larger PAH clusters having 100-1000 C atoms (see e.g. Rapacioli, Joblin & Boissel 2005; Berné et al. 2008).

It would therefore appear that a multiplicity of mechanisms might cause variations in relative PAH emission band strengths, and explain the differences in the MIR colour planes noted in this work. Broadly speaking, where the properties of grain populations vary, and/or conditions of ionisation are modified, then one might expect corresponding changes in relative PAH band strengths.

Such variations in grain properties might be expected to occur where there are changes in source metallicity, such as appear to arise between the LMC and Galactic PN outflows (see our comments in Sect. 1), whilst one might also expect to observe differences in underlying

levels of grain continuum emission; in central star properties (see e.g. the evolutionary curves of Vassiliadis & Wood (1994) for differing progenitor metallicities); in line emission characteristics, and, conceivably, in the masses of the nebular shells.

Thus for instance, given that dust/gas mass ratios appear to be surprisingly similar for all metallicities of outflow (see e.g. Phillips 2007), then it is arguable that Magellanic sources would show a higher level of elemental depletion – that is, an increase in the fractional masses of heavier elements which are contained within the dust, and a corresponding reduction in gas phase abundances for the lower metallicity sources (Phillips 2007). This would likely lead to corresponding changes in the permitted and forbidden line spectra.

Similarly, differences in metallicity would plausibly influence grain formation properties within the flows (see e.g. the discussion by Ferrarotti & Gail (2006) of dust formation in C- and O-rich environments, and Sedlmayr & Dominik (1995) for the physics and chemistry involved radiatively driven outflows), and this may account for the lower fractional masses of PAH type grains in lower metallicity environments (see e.g. Draine et al. 2007).

Further testing of such hypotheses is possible through MIR spectroscopy of the sources, and it would be of interest to obtain a larger sample of such observations than is currently available.

Finally, and as mentioned above, it is fascinating to note that [4.5]-[8.0] indices for LMC and Galactic nebulae are reasonably similar. This is perhaps somewhat unexpected given our discussion above – although it is possible that a combination of lower shell masses and PAH fractional masses may lead to compensating reductions in 4.5 and 8.0 μm emission, and comparable values for [4.5]-[8.0].

7. Conclusions

We have undertaken a comparative analysis of the magnitudes and colours of GBPNe, GDPNe and LMC PNe based upon data products deriving from the GLIMPSE II and SAGE Galactic Legacy Programs. This has permitted us to determine that the 3.6 μm luminosity function for LMC PNe is similar to that of their Galactic bulge counterparts –

and within the uncertainties engendered by incompleteness of the LMC sample. The colour-colour distributions of the sources are also for the most part similar, although with differences (in the case of [3.6]-[4.5]) arising from incompleteness of the LMC sample.

The only exceptions to this trend appear to be in the [4.6]-[5.8] and [5.8]-[8.0] indices. The LMC nebulae tend to be confined to higher values of the [4.6]-[5.8] index, for instance – much larger than is the case for the bulge and disk PNe. By contrast, the [5.8]-[8.0] index tends to be significantly lower. This difference between the LMC and Galactic sources may arise due to enhanced PAH band emission within the 5.8 μm photometric channel, suggesting that the nature of PAH excitation, or of the PAH grains themselves, may differ between these differing categories of source. Alternatively, such a situation may reflect the fact that a large proportion of LMC nebulae appear to contain very little MIR dust emission at all, leading to a dominance by permitted and forbidden line fluxes, stellar continua, and bremsstrahlung emission.

Previous analyses of MASH sources appeared to indicate that many of them were located within a highly restricted regime of the [3.6]-[4.5]/[5.8]-[8.0] colour plane; a regime which was much more constrained than that of less evolved GDPNe, such as the sources listed in the catalogue of Acker et al. (1992).

Our present results do not confirm this trend, but rather indicate that the Acker et al. (1992) and MASH sources have similar colours.

Acknowledgements

We would like to thank an anonymous referee for several very useful insights. This referee also suggested removing a large section of mapping data relating to the present sources; data which will now be published in a further article concerning GLIMPSE II and 3D PNe. This work is based, in part, on observations made with the Spitzer Space Telescope, which is operated by the Jet Propulsion Laboratory, California Institute of Technology under a contract with NASA. Support for this work was provided by an award issued by JPL/Caltech. It also makes use of data products from the Two Micron All Sky Survey, which is a joint project of the University of Massachusetts and the Infrared

Processing and Analysis Center/California Institute of Technology, funded by the National Aeronautics and Space Administration and the National Science Foundation. GRL acknowledges support from CONACyT (Mexico) grant 93172.

References

- Acker A., Ochsenbein F., Stenholm B., Tyllenda R., Marcout J., Schohn C., 1992, Strasbourg-ESO Catalogue of Planetary Nebulae, ESO, Garching
- Acker A., Peyaud A. E. J., Parker Q., 2006, in Barlow M.J., Méndez R.H., eds, , Proc. IAU Symp. 234, Planetary Nebulae in our Galaxy and Beyond. C.U.P., Cambridge, p.355
- Allamandola L. J., Huggins D. M., Sandford S. A., 1999, ApJ, 511, 115
- Amnuel P.R., 1993, MNRAS, 261, 263
- Andersen A. C., Jaéger C., Mutschke H., Braatz A., Cleament D., Henning Th., Jürgensen U. G., Ott U., 1999, A&A, 343, 933
- Beaulieu S.F., Dopita M.A., Freeman K.C., 1999, ApJ, 515, 610
- Benjamin R. A., Churchwell E., Babler B. L., Bania T. M., Clemens D. P., Cohen M., Dickey J. M., Indebetouw R., Jackson J. M., Kobulnicky H. A., et al., 2003, PASP, 115, 953
- Berné O., Joblin C., Rapacioli M., Thomas J., Cuillandre J-C, Deville Y., 2008. A&A, 479, L41
- Bernard-Salas J., Houck J. R., Pottasch S. R., Peeters E., 2005, in Szczerba R., Stasínska G., Górny S. K., eds, AIP Conf. Proc. 804, Planetary Nebulae as Astronomical Tools. AIP, New York, p. 56
- Cahn J.H., Kaler J.B., 1971, ApJS, 22, 319
- Cardelli J.A., Clayton G.C., Mathis J.S., 1989, ApJ, 345, 245
- Casassus S., Roche P.F., Aitken D.K., Smith C.H., 2001, MNRAS, 320, 424
- Chiappini C., Górny S.K., Stasínska G., Barbuy B., 2008, preprint (astro-ph/0812.0558v)

Cohen M., Green A.J., Meade M.R., Babler B., Indebetouw R., Whitney B.A., Watson C., Wolfire M., Wolff M.J., Mathis J.S., Churchwell E.B., 2007a, MNRAS, 374, 979

Cohen M., Parker Q.A., Green A. J., Murphy T., Miszalski B., Frew D.J., Meade M. R., Babler B., Indebetouw R., Whitney B. A., Watson C., Churchwell E. B., Watson D.F., 2007b, ApJ, 669, 343

Corradi R.L.M., Schwarz H.E., 1993, A&A, 269, 462

Corradi R.L.M., Sánchez-Blázquez, Mellema, P.G., Gianmanco C., Schwarz H.E., 2004, A&A, 417, 637

Cuisinier F., Köppen J., Acker A., Maciel W. J., 2002, RMxAC, 12, 136

Draine B.T., 2003, ARA&A, 41, 241

Draine B.T., Dale D.A., Bendo G., Gordon K.D., Smith J.D.T., et al. 2007, ApJ, 663, 866

Eisenhauer F., Genzel R., Alexander T., Abuter R., Paumard T., Ott T., Gilbert A., Gillessen S., Horrobin M., Trippe S., Bonnet H., Dumas C., Hubin N., Kaufer A., Kissler-Patig M., Monnet G., Ströbele S., Szeifert T., Eckart A., Schödel R., Zucker S., 2005, ApJ, 628, 246

Fazio G. G., Hora J. L., Allen L. E., Ashby M. L. N., Barmby P., Deutsch L. K., Huang J.-S., Kleiner S., Marengo M., Megeath S. T., Melnick G. J., Pahre M. A., Patten B. M., Polizotti J., Smith H. A., Taylor R. S., Wang Z., Willner S. P., Hoffmann W. F., Pipher J. L., Forrest W. J., McMurty C. W., McCreight C. R., McKelvey M. E., McMurray R. E., Koch D. G., Moseley S. H., Arendt R. G., Mentzell J. E., Marx C. T., Losch P., Mayman P., Eichhorn W., Krebs D., Jhabvala M., Gezari D. Y., Fixsen D. J., Flores J., Shakoorzadeh K., Jungo R., Hakun C., Workman L., Karpati G., Kichak R., Whitley R., Mann S., Tollestrup E. V., Eisenhardt P., Stern D., Gorjian V., Bhattacharya B., Carey S., Nelson B. O., Glaccum W. J., Lacy M., Lowrance P. J., Laine S., Reach W. T., Stauffer J. A., Surace J. A., Wilson G., Wright E. L., Hoffman A., Domingo G., Cohen M., 2004, ApJS, 154, 10

Faundez-Abans M., Maciel W.J., 1986, A&A, 158, 228

Fleischer A.J., Gauger A., Sedlmayr E., 1992, A&A, 266, 321

Forrest W.J., Gillett F.C., Stein W.A., 1975, ApJ, 195, 423

Gauger A., Gail H.-P., Sedlmayr W., 1990, A&A, 235, 345

Gillessen S., Eisenhauer F., Trippe S., Alexander T., Genzel R., Martins F., Ott T., 2008, preprint (astro-ph/0810.4674v1)

Gordon K.D., Clayton G.C., Misselt K. A., Landolt A.U., Wolff M.J., 2003, ApJ, 594, 279

Górny S.K., Stasińska G., Escudero A.V., Costa R.D.D., 2004, A&A, 427, 231

Gutenkunst S., Bernard-Salas J., Pottasch S. R., Sloan G. C., Houck J. R., 2008, ApJ. 680, 1206

Helling Ch., Arndt T.U., Sedlmayr E., 2002, in Aerts C., Bedding T.R., Christensen-Dalsgaard J., eds, ASP Conf. Ser. 259, IAU Colloq. 185, Radial and Non-Radial Pulsations as Probes of Stellar Physics. Astron. Soc. Pac., San Francisco, p. 546

Hollenbach D.J., Tielens A.G.G.M., 1997, ARA&A, 35, 179

Hora J. L., Cohen M., Ellis R. G., Meixner M., Blum R. D., Latter W. B., Whitney B. A., Meade M. R., Babler B. L., Indebetouw R., et al., 2008, AJ, 135, 726

Hora J.L., Latter W.B., Allen L.E., Marengo M., Deutsch L.K., Pipher J.L., 2004, ApJS, 154, 296

Indebetouw R., Mathis J.S., Babler B.L., Meade M.R., Watson C., Whitney B.A., Wolff M.J., Wolfire M.G., Cohen M., Bania T.M., Benjamin R.A., Clemens D.P., Dickey J.M., Jackson J.M., Kobulnicky H.A., Marston A.P., Mercer E.P., Stauffer J.R., Stolovy S.R., Churchwell E., 2005, ApJ, 619, 931

- Kinman T.D., Feast M.W., Lasker B.M., 1988, AJ, 95, 804
- Koppen J., Acker A., Stenholm B., 1991, A&A, 248, 197
- Leger A., D'Hendecourt L. B., 1988, in Bailey M.E., Williams D.A., eds, Dust in the Universe, C.U.P., Cambridge, p. 219
- Leisy P., Dennefeld M., Alard C., Guibert J., 1997, A&A, 121, 407
- Maciel W.J., Costa R. D. D., Idiart T.E.P., 2006, in Stanghellini L., Walsh J. R., Douglas N.G., eds., Planetary Nebulae beyond the Milky Way. Springer, Berlin, p. 209
- Maciel W.J., Costa R.D.D., Idiart T.E.P., 2008, in van Loon J. Th., Oliveira J. M., eds, Proc. IAU Symp. 256, The Magellanic System: Stars, Gas, and Galaxies. C.U.P. Cambridge, in press
- Maciel W.J., Koppen J., 1994, A&A, 282, 436
- Maciel W.J., Quireza C., 1999, A&A, 345, 629
- Macri L.M., Stanek K.Z., Bersier D., Greenhill L.J., Reid M.J., 2006, ApJ, 652, 1133
- Martins L. P., Viegas S. M. M., 2000, A&A, 361, 1121
- Meixner M., et al. 2006, AJ, 132, 2268
- Miszalski B., Parker Q. A., Acker A., Birkby J. L., Frew D. J., Kovacevic A., 2008, MNRAS, 384, 525
- Molster F.J., Waters L.B.F.M., Tielens A.G.G.M., 2002, A&A, 382, 222
- Moreno H., Lasker B.M., Gutierrez-Moreno A., Torres C., 1988, PASP, 100, 604
- O'Dell C. R., Balick B., Hajian A. R., Henney W. J., Burkert A. 2002, AJ, 123, 3329
- O'Dell C.R., Balick B., Hajian A. R., Henney W.J., Burkert A., 2002, RMxAC, 15, 29

Peeters E., Hony S., Van Kerckhoven C., Tielens A. G. G. M., Allamandola L. J., Hudgins D. M., Bauschlicher C. W., 2002, *A&A*, 390, 1089

Parker Q. A., Acker A., Frew D. J., Hartley M., Peyaud A. E. J., Ochsenbein F., Phillipps S., Russeil D., Beaulieu S. F., Cohen M., Köppen J., Miszalski B., Morgan D. H., Morris R. A. H., Pierce M. J., Vaughan A. E., 2006, *MNRAS*, 373, 79

Parker Q. A., Phillipps S., Pierce M. J., Hartley M., Hambly N. C., Read M. A., MacGillivray H. T., Tritton S. B., Cass C. P., Cannon R. D., Cohen M., Drew J. E., Frew D. J., Hopewell E., Mader S., Malin D. F., Masheder M. R. W., Morgan D. H., Morris R. A. H., Russeil D., Russell K. S., Walker R. N. F., 2005, *MNRAS*, 362, 689

Pasquali A., Perinotto M., 1993, *A&A*, 280, 581

Peimbert M., Torres-Peimbert S., 1983, in Flower R., ed., *Proc. IAU Symp. No. 193, Planetary Nebulae*. D. Reidel Publishing Co., Dordrecht, Holland, p. 233

Perea-Calderón J.V., García-Hernández D.A., García-Lario P., Szczerba R., Bobrowsky M., 2009, arxiv.org/abs/0902.1049

Phillips J.P., 2003, *MNRAS*, 344, 501

Phillips J.P., 2007, *MNRAS*, 381, 117

Phillips J.P., Ramos-Larios G., 2008a, *MNRAS*, 383, 1029

Phillips J.P., Ramos-Larios G., 2008b, *MNRAS*, 386, 995

Phillips J.P., Ramos-Larios G., 2008c, *MNRAS*, 391, 1527

Phillips J.P., Perez-Grana A., 2009, *MNRAS*, in press

Pishmish P., Manteiga M., Mampaso Recio A. 2000, in Kastner J. H., Soker N, Rappaport S., eds, *ASP Conf. Ser. Vol. 199, Asymmetrical*

Planetary Nebulae II: From Origins to Microstructures. Astron. Soc. Pac., San Francisco, p. 397

Pottasch S.R., Acker A., 1989, A&A, 221, 123

Pottasch S. R., Surendiranath R., 2007, A&A, 462, 179

Ramos-Larios G., Phillips J.P., 2005, MNRAS, 357, 732

Ramos-Larios G., Phillips J.P., 2008a, MNRAS, 390, 1014

Ramos-Larios G., Phillips J.P., 2008b, MNRAS, 391, 52

Rapacioli M., Joblin C., Boissel P., 2005. A&A, 429, 193

Reach W. T., Megeath S. T., Cohen M., Hora J., Carey S., Surace J., Willner S. P., Barmby P., Wilson G., Glaccum W., Lowrance P., Marengo M., Fazio G. G., 2005, PASP, 117, 978

Reid W.A., Parker Q.A., 2006, MNRAS, 373, 521

Rieke G. H., et al., 2004, ApJS, 154, 25

Ruffle P.M.E., Zijlstra A.A., Walsh J.R., Gray M.D., Gesicki K., Minniti D., Comeron F., 2004, MNRAS, 353, 796

Samland M., Koppen J., Acker A., Stenholm B., 1992, A&A, 264, 184

Schonberner D., 1981, A&A, 103, 119

Sedlmayr E., Dominik C., 1995, Space Science Reviews, 73, 211

Stanghellini L., García-Lario P., García-Hernández D.A., Perea-Calderón J.V., Davies J.E., Manchado A., Villaver E., Shaw R.A., 2007, ApJ, 671, 1669

Su K. Y. L., Chu Y.-H., Rieke G. H., Huggins P. J., Gruendl R., Napiwotzki R., Rauch T., Latter W. B., Volk K., 2007, ApJ, 657, 41

Su K.Y.L., Kelly D.M., Latter W.B., Misselt K.A., Frank A., Volk K., Engelbracht C.W., Gordon K.D., Hines W.C., Morrison J.D., et al., 2004, ApJS, 154, 302

Tielens A.G.G.M., 2005, The Physics and Chemistry of the Interstellar Medium, C.U.P., Cambridge

Tielens A.G.G.M., 2008, ARA&A, 46, 289

Tokunaga A.T., 2000, in Cox A.N., ed., Allen's Astrophysical Quantities. Springer, New York

Ueta T., 2006, ApJ, 650, 228

Van de Steene G.C., Jacoby G.H., 2001, A&A, 373, 536

Vassiliadis E., Wood P.R., 1994, ApJS, 92, 125

Villaver E., Stanghellini L., Shaw R.A., 2003, ApJ, 597, 298

Villaver E., Stanghellini L., Shaw R.A., 2004, 614, 716

Wachter A., Winters J. M., Schröder K.-P., Sedlmayr E., 2007, A&A, 486, 497

Wachter A., Schroder K.-P., Winters J.M., Arndt T.U., Sedlmayr E., 2002, A&A, 384, 452

Walton N. A., Barlow, M. J., Clegg, R. E. S. 1993, in H. Dejonghe, H., Habing H. J., eds, IAU Symp. 153, Galactic Bulges. Kluwer Academic Publishers, Dordrecht, Holland, p. 337

Wang W., Liu X.-W., 2007, MNRAS, 381, 669

Waters L.B.F.M., Beintema D.A., Zijlstra A.A., et al., 1998, A&A, 331, L61

Werner M.W., et al. 2004, ApJS, 154, 1

Winters J.M., Fleischer A.J., Gauger A., Sedlmayr E., 1994, A&A, 290, 623

Winters J.M., Le Bertre T., Jeong K.S., Helling Ch., Sedlmayr E., 2000, A&A, 361, 641

Winters J.M., LeBertre T., Jeong K.S., Nyman L.-Å, Epchtein N., 2003 , A&A, 409, 715

Zijlstra A.A., 2007, Baltic Astron., 16, 79

Zijlstra A.A., Pottasch S.R., Bignell C., 1989, A&AS, 79, 329

Table 1

MIR Photometry of Acker and MASH Planetary Nebulae

G.C.	CAT.	NAME	[3.6] mag	$\sigma_{3.6}$ mag	[4.5] mag	$\sigma_{4.5}$ mag	[5.8] mag	$\sigma_{5.8}$ mag	[8.0] mag	$\sigma_{8.0}$ mag
G000.0-01.3	MASHI	PPA1751-2933	12.92	0.05	12.08	0.04	10.73	0.10	7.31	0.01
G000.1-01.7	MASHI	PHR1752-2941	11.71	0.08	11.37	0.02	11.52	0.07	7.92	0.01
G000.1-01.1	ACK	M 3-43	10.43	0.30	9.53	0.09	8.29	0.07	5.85	0.06
G000.1+01.9	MASHI	PHR1738-2748	11.51	0.03	11.68	0.05	11.69	0.06	11.20	0.23
G000.2-01.9	ACK	M 2-19	10.65	0.14	10.83	0.13	9.94	0.09	9.00	0.01
G000.4-01.9	ACK	M 2-20	10.16	0.11	9.80	0.12	9.18	0.06	7.13	0.06
G000.5-01.6	ACK	AI 2-Q	12.54	0.05	11.82	0.03	12.92	0.06	10.12	0.01
G000.6-01.3	ACK	BI 3-15	10.20	0.02	10.55	0.02	9.59	0.01	8.48	0.02
G000.8-01.5	ACK	BI O	10.95	0.02	11.06	0.01	9.47	0.01	8.14	0.02
G000.9-02.0	ACK	BI 3-13	12.67	0.14	11.36	0.11	11.86	0.05	8.71	0.09
G001.0-01.9	MASHI	PHR1755-2904	13.58	0.38	11.36	0.01	11.76	0.04	7.39	0.02
G001.0+01.9	ACK	K 1- 4	9.67	0.04	9.65	0.05	9.69	0.06	9.59	0.03
G001.1-01.6	ACK	Sa 3- 92	11.86	0.01	12.30	0.03	12.56	0.04	10.88	0.01
G001.1-01.2	MASHI	PPA1753-2836	7.89	0.02	8.15	0.02	7.89	0.02	7.07	0.02
G001.3-01.2	ACK	BI M	11.12	0.04	10.91	0.01	10.41	0.02	8.77	0.02
G001.7-01.6	ACK	H 2-31	11.36	0.11	10.63	0.07	9.52	0.06	7.38	0.06
G002.1-00.9	MASHI	PHR1754-2736	10.16	0.02	9.46	0.02	8.54	0.02	5.59	0.02
G002.2-01.2	MASHI	PPA1755-2739	13.10	0.08	11.25	0.01	10.82	0.05	7.11	0.01
G002.2+00.5	ACK	Te 2337	10.48	0.02	9.42	0.02	8.02	0.02	4.99	0.02
G003.5+01.3	MASHII	MPA1748-2511	12.25	0.01	10.87	0.01	11.27	0.03	9.33	0.02
G003.6-01.3	MASHI	PHR1759-2630	11.20	0.01	10.14	0.03	10.05	0.01	7.25	0.02
G004.0-00.4	MASHI	PHR1756-2538	---	---	9.19	0.02	8.88	0.04	7.34	0.01
G004.3-01.4	MASHI	PPA1801-2553	12.09	0.02	11.11	0.01	11.09	0.08	7.40	0.01
G004.8-01.1	MASHI	PHR1801-2522	10.47	0.02	9.39	0.01	9.20	0.05	5.85	0.01
G006.1+00.8	MASHI	PPA1756-2311	12.71	0.08	11.94	0.04	12.24	0.03	7.20	0.02
G006.2+01.0	ACK	HaTr 8	13.20	0.10	12.54	0.16	12.15	0.10	10.54	0.04
G008.6+01.0	MASHI	PHR1801-2057	---	---	12.38	0.04	---	---	7.04	0.02
G352.6+00.1	ACK	H 1-12	8.14	0.02	7.59	0.02	7.82	0.02	6.42	0.02
G352.8-00.5	MASHII	MPA1729-3513	9.47	0.01	8.39	0.02	7.45	0.02	5.99	0.02
G352.8-00.2	ACK	H 1-13	8.16	0.02	7.57	0.02	7.88	0.02	6.13	0.01
G353.9+00.0	MASHI	PPA1730-3400	9.55	0.01	8.98	0.02	8.48	0.01	7.53	0.01
G355.6+01.4	MASHI	PPA1729-3152	11.46	0.01	10.47	0.02	9.27	0.02	7.23	0.02
G356.0-01.4	MASHI	PPA1741-3302	13.01	0.06	11.51	0.03	11.68	0.11	8.30	0.01
G356.5+01.5	ACK	Th 3-55	12.12	0.02	11.53	0.02	11.63	0.03	9.99	0.02
G356.9+00.9	MASHI	PPA1734-3102	10.33	0.02	10.10	0.01	8.36	0.01	6.17	0.02
G357.2+01.4	ACK	AI 2-H	13.78	0.16	12.63	0.06	12.94	0.12	11.34	0.11
G357.5+01.3	MASHI	PPA1734-3015	11.61	0.02	11.27	0.03	9.04	0.01	7.15	0.01
G358.2-01.1	ACK	BI D	10.72	0.02	9.86	0.02	9.72	0.02	8.05	0.02
G358.3+01.2	ACK	BI B	10.56	0.01	10.59	0.02	9.72	0.01	8.21	0.01
G358.8-00.0	ACK	Te 2022	5.50	0.02	5.37	0.02	2.37	0.02	0.55	0.02
G359.1-01.7	ACK	M 1-29	9.79	0.02	8.96	0.01	9.03	0.02	7.34	0.02
G359.2+01.2	ACK	19W32	8.83	0.01	8.84	0.02	6.93	0.02	6.19	0.02
G359.3+01.4	ACK	Th 3-35	10.92	0.10	9.62	0.07	8.95	0.05	6.55	0.04
G359.3-00.9	ACK	Hb 5	7.30	0.02	6.30	0.02	5.02	0.02	2.82	0.02
G359.3-01.8	ACK	M 3-44	10.39	0.23	9.88	0.13	8.23	0.07	6.57	0.14
G359.7-01.8	ACK	M 3-45	11.87	0.02	11.03	0.02	11.24	0.06	10.83	0.04

Table 2

MIR Photometry of the Galactic Bulge Planetary Nebulae
of Van de Steene & Jacoby (2001)

G.C.	JaSt	[3.6] mag	$\sigma_{3.6}$ mag	[4.5] mag	$\sigma_{4.5}$ mag	[5.8] mag	$\sigma_{5.8}$ mag	[8.0] mag	$\sigma_{8.0}$ mag
G000.01-1.80	83	---	---	11.09	0.20	---	---	11.16	0.14
G000.05+1.29	27	11.20	0.05	11.26	0.09	10.99	0.07	10.18	0.14
G000.08-0.93	67	11.87	0.19	10.77	0.24	10.67	0.24	8.92	0.05
G000.10-1.91	93	13.71	0.09	13.30	0.11	13.58	0.22	10.68	0.03
G000.15-1.73	85	11.61	0.00	11.79	0.11	12.21	0.05	10.88	0.02
G000.17-1.21	75	11.61	0.10	10.72	0.11	10.37	0.08	8.49	0.05
G000.18-1.04	69	11.31	0.11	10.67	0.07	10.37	0.08	9.64	0.06
G000.20-1.47	79	5.08	0.09	4.82	0.09	3.91	0.03	3.40	0.05
G000.28+1.71	19	13.07	0.11	12.70	0.27	12.34	0.04	11.48	0.04
G000.33-1.64	86	12.59	0.06	11.84	0.07	12.63	0.21	11.00	0.01
G000.34+1.56	23	11.86	0.09	10.49	0.07	8.77	0.04	6.08	0.04
G000.35+1.70	21	10.28	0.05	10.38	0.06	10.44	0.08	10.27	0.06
G000.39+0.63	49	12.51	0.04	12.38	0.04	12.27	0.03	10.83	0.02
G000.49+1.12	36	11.77	0.13	10.80	0.10	10.43	0.10	9.83	0.11
G000.54+1.91	17	12.90	0.08	12.06	0.03	12.86	0.12	10.12	0.01
G000.59-1.76	96	9.89	0.06	10.01	0.08	10.01	0.06	9.93	0.05
G000.62-1.04	77	10.17	0.12	9.29	0.05	8.92	0.04	6.49	0.04
G000.74-0.86	74	12.08	0.15	11.10	0.13	11.05	0.15	9.52	0.12
G000.78-0.74	70	11.82	0.05	11.10	0.01	12.20	0.11	10.29	0.00
G000.82+1.30	38	12.28	0.15	12.24	0.13	11.53	0.23	10.30	0.06
G000.86-0.69	71	---	---	10.14	0.12	---	---	8.06	0.08
G000.90+1.13	44	12.58	0.10	12.43	0.15	12.39	0.24	9.85	0.14
G000.94-0.91	78	12.04	0.01	11.59	0.01	12.41	0.04	11.23	0.01
G000.95-0.78	76	12.82	0.11	11.17	0.09	11.12	0.08	10.27	0.08
G001.02+1.35	41	12.19	0.12	11.51	0.16	10.86	0.11	9.41	0.09
G001.13+0.80	54	8.89	0.00	8.41	0.00	5.95	0.00	3.89	0.00
G001.17+1.68	34	13.62	0.14	13.21	0.17	11.97	0.29	9.22	0.01
G001.23+0.71	56	11.41	0.12	11.09	0.17	10.89	0.18	9.85	0.26
G001.23+1.33	45	13.17	0.10	13.11	0.12	---	---	---	---
G001.28-1.26	95	13.17	0.10	12.13	0.11	13.23	0.07	10.35	0.01
G001.38-1.08	89	12.29	0.07	11.97	0.02	12.77	0.03	11.39	0.06
G001.58+1.51	46	11.83	0.09	10.59	0.06	10.08	0.05	7.76	0.04
G001.60-1.00	90	11.00	0.11	11.02	0.12	10.40	0.10	9.98	0.19
G001.60+1.58	42	12.43	0.02	11.71	0.24	11.32	0.13	8.26	0.06
G001.71+1.30	52	11.11	0.05	10.37	0.06	10.18	0.06	7.77	0.03
G001.86-0.53	81	11.05	0.06	9.95	0.05	9.05	0.06	7.15	0.03
G002.03-1.38	98	10.91	0.03	9.97	0.05	8.47	0.02	6.43	0.02
G358.02+1.56	1	13.31	0.17	13.07	0.06	13.60	0.16	12.35	0.01
G358.17+0.55	11	12.84	0.05	12.78	0.05	12.68	0.07	10.63	0.16
G358.31+0.27	24	11.71	0.01	11.55	0.03	11.70	0.03	9.86	0.01
G358.40+1.73	2	12.50	0.15	12.30	0.16	10.87	0.09	10.30	0.01
G358.44+1.66	3	12.70	0.12	12.06	0.25	11.22	0.14	11.02	0.04
G358.51-1.74	64	10.34	0.04	9.38	0.05	8.63	0.03	7.01	0.03
G358.60+1.70	4	14.01	0.22	12.88	0.06	13.97	0.19	11.18	0.05
G358.63+0.75	16	11.88	0.16	10.65	0.16	10.92	0.16	8.78	0.21

Table 2 (cont.)

G.C.	JaSt	[3.6] mag	$\sigma_{3.6}$ mag	[4.5] mag	$\sigma_{4.5}$ mag	[5.8] mag	$\sigma_{5.8}$ mag	[8.0] mag	$\sigma_{8.0}$ mag
G358.69-1.11	58	12.49	0.07	11.87	0.07	11.56	0.05	9.69	0.06
G358.71+0.49	26	12.90	0.10	12.21	0.09	11.53	0.06	9.95	0.11
G358.83+1.78	5	12.97	0.07	12.02	0.02	11.94	0.08	11.72	0.02
G358.99-1.55	65	10.86	0.05	9.85	0.05	9.16	0.04	5.58	0.04
G359.02+1.16	9	12.66	0.07	11.83	0.02	11.90	0.06	10.03	0.07
G359.23+1.36	8	13.79	0.25	12.72	0.07	13.68	0.07	10.79	0.01
G359.29+1.41	7	11.89	0.09	11.72	0.09	11.68	0.14	11.81	0.14
G359.52-1.36	68	12.12	0.07	11.10	0.07	10.46	0.08	7.39	0.04
G359.52-1.24	66	10.92	0.19	10.20	0.13	9.56	0.07	8.62	0.06
G359.57+0.80	31	12.28	0.02	11.93	0.04	12.42	0.07	10.08	0.07
G359.67-0.77	60	9.80	0.05	8.84	0.09	7.42	0.03	5.35	0.04
G359.76-1.45	73	11.27	0.02	11.21	0.18	10.76	0.10	8.53	0.05

Table 3

2MASS and Spitzer Photometry for the LMC Planetary Nebulae of Reid & Parker (2006)

#	/	b	deg	NAME	STAT	J	σ_J	H	σ_H	K _S	σ_{K_S}	[3.6]	$\sigma_{3.6}$	[4.5]	$\sigma_{4.5}$	[5.8]	$\sigma_{5.8}$	[8.0]	$\sigma_{8.0}$	r	
						mag	mag	mag	mag	mag	mag	mag	mag	mag	mag	mag	mag	mag	mag	mag	arcs
4	280.992	-35.4229	RPJ 045403-693320	T	17.46	0.10	16.87	0.12	---	---	15.99	0.10	15.50	0.11	---	---	---	---	---	---	0.76
6	280.727	-35.4454	RPJ 045433-692035	P	14.36	0.04	13.59	0.02	12.41	0.03	9.95	0.03	8.94	0.05	8.02	0.03	6.65	0.03	6.65	0.03	0.66
14	277.724	-35.8697	RPJ 045733-665258	T	---	---	---	---	---	---	16.67	0.12	15.67	0.08	14.35	0.17	12.53	0.06	1.20	---	1.20
15	280.875	-35.1052	RPJ 045751-693333	T	---	---	---	---	---	---	16.74	0.11	15.96	0.11	---	---	---	---	---	---	0.88
16	280.499	-35.1939	RPJ 045754-691421	T	---	---	---	---	---	---	---	---	16.24	0.16	---	---	---	---	---	---	1.17
25	278.158	-35.5662	RPJ 045937-671805	T	---	---	---	---	---	---	16.37	0.14	16.48	0.14	---	---	---	---	---	---	1.69
27	281.325	-34.7532	RPJ 050032-700049	P	17.37	0.13	16.31	0.11	15.26	0.07	12.81	0.06	11.97	0.03	10.88	0.04	9.15	0.03	0.69	---	0.69
28	282.316	-34.5041	RPJ 050034-705200	T	---	---	15.22	0.05	---	---	10.45	0.03	9.60	0.02	8.97	0.03	8.31	0.02	0.74	---	0.74
30	279.879	-35.0638	RPJ 050052-684717	T	---	---	---	---	---	---	17.10	0.14	---	---	---	---	---	---	---	---	1.58
31	279.099	-35.229	RPJ 050058-680748	T	---	---	---	---	---	---	15.25	0.09	14.51	0.11	13.17	0.09	11.26	0.09	0.67	---	0.67
32	279.209	-35.1891	RPJ 050108-681337	T	16.27	0.06	15.70	0.07	15.66	0.11	15.71	0.11	15.85	0.14	---	---	---	---	---	---	1.91
37	280.284	-34.8602	RPJ 050203-690945	T	---	---	---	---	---	---	16.54	0.13	15.86	0.15	---	---	13.55	0.11	0.70	---	0.70
38	278.394	-35.2731	RPJ 050204-673343	T	---	---	---	---	---	---	16.55	0.09	15.73	0.11	---	---	---	---	---	---	1.23
39	280.166	-34.8679	RPJ 050216-690403	T	---	---	---	---	---	---	15.91	0.14	---	---	---	---	---	---	---	---	2.25
40	279.468	-35.0006	RPJ 050230-682848	T	---	---	---	---	---	---	16.42	0.10	---	---	---	---	---	---	---	---	0.28
43	281.383	-34.5041	RPJ 050311-700744	T	16.77	0.08	15.88	0.08	14.98	0.07	14.11	0.08	13.73	0.06	13.14	0.09	12.75	0.07	0.54	---	0.54
45	280.116	-34.7408	RPJ 050345-690341	P	---	---	---	---	---	---	14.28	0.10	13.37	0.05	12.58	0.07	11.55	0.06	0.44	---	0.44
47	279.99	-34.7596	RPJ 050351-685723	T	13.97	0.03	13.89	0.03	13.71	0.03	13.20	0.05	13.06	0.05	12.71	0.06	---	---	---	---	0.82
48	282.507	-34.1438	RPJ 050415-710717	P	17.58	0.10	16.87	0.13	---	---	16.75	0.08	16.71	0.18	---	---	---	---	---	---	0.68
50	278.417	-35.0449	RPJ 050421-673809	T	17.43	0.09	16.89	0.13	16.66	0.21	16.74	0.10	16.69	0.14	---	---	---	---	---	---	1.25
51	282.117	-34.225	RPJ 050424-704719	P	---	---	---	---	---	---	14.93	0.08	14.07	0.07	12.80	0.12	---	---	---	---	1.96
52	280.403	-34.6064	RPJ 050431-691928	T	---	---	16.40	0.10	14.25	0.04	11.76	0.05	10.97	0.03	10.26	0.04	9.53	0.04	1.07	---	1.07
53	278.691	-34.9676	RPJ 050434-675221	T	16.39	0.04	15.27	0.03	14.33	0.04	12.49	0.03	11.74	0.03	11.04	0.03	10.13	0.03	0.18	---	0.18
54	281.316	-34.3962	RPJ 050435-700618	T	---	---	---	---	---	---	15.05	0.17	14.67	0.08	12.39	0.14	---	---	---	---	0.31
56	277.45	-35.2046	RPJ 050440-664947	P	16.14	0.03	16.06	0.06	16.23	0.16	16.12	0.13	---	---	---	---	---	---	---	---	1.22

Table 3 (cont.)

#	l deg	b deg	NAME	STAT	J mag	σ_J mag	H mag	σ_H mag	Ks mag	σ_{Ks} mag	[3.6] mag	$\sigma_{3.6}$ mag	[4.5] mag	$\sigma_{4.5}$ mag	[5.8] mag	$\sigma_{5.8}$ mag	[8.0] mag	$\sigma_{8.0}$ mag	r arcs
106	280.562	-33.9021	RPJ 051157-693729	P	14.72	0.02	14.38	0.03	14.18	0.04	13.66	0.06	13.38	0.05	13.25	0.09	11.91	0.08	2.36
109	279.91	-33.9749	RPJ 051232-690452	T	---	---	---	---	---	---	16.13	0.09	---	---	---	---	---	---	1.29
111	280.627	-33.8101	RPJ 051250-694152	P	16.67	0.06	16.32	0.11	15.93	0.14	14.67	0.06	14.22	0.08	13.43	0.11	---	---	0.69
114	280.387	-33.7953	RPJ 051331-693025	T	15.43	0.04	14.81	0.04	14.81	0.06	14.62	0.07	14.76	0.10	---	---	---	---	1.70
115	277.82	-34.2186	RPJ 051353-672017	P	15.13	0.06	13.83	0.05	12.59	0.04	10.51	0.06	9.81	0.04	8.60	0.04	7.32	0.08	1.81
118	281.688	-33.4924	RPJ 051404-703751	T	16.52	0.05	16.11	0.08	15.83	0.13	15.52	0.11	15.23	0.14	---	---	---	---	0.08
119	282.029	-33.4133	RPJ 051412-705533	T	17.18	0.08	16.62	0.12	16.37	0.19	16.44	0.10	16.15	0.12	---	---	---	---	2.13
120	279.28	-33.9204	RPJ 051423-683456	T	---	---	---	---	---	---	16.51	0.10	---	---	---	---	---	---	2.32
121	280.136	-33.7257	RPJ 051449-691908	T	14.35	0.03	13.73	0.03	13.52	0.03	13.36	0.04	13.45	0.05	13.33	0.12	---	---	0.40
123	279.303	-33.8512	RPJ 051505-683655	T	---	---	---	---	---	---	16.34	0.11	15.83	0.08	13.58	0.11	11.78	0.06	0.53
125	278.691	-33.9004	RPJ 051540-680628	L	14.28	0.03	13.67	0.03	13.44	0.03	13.09	0.03	13.03	0.03	12.97	0.06	13.11	0.10	0.95
127	279.443	-33.7487	RPJ 051555-684503	T	16.28	0.05	15.62	0.05	15.49	0.09	15.32	0.06	15.34	0.09	---	---	---	---	2.09
128	280.134	-33.6029	RPJ 051611-692036	T	15.03	0.04	14.53	0.04	14.34	0.04	14.45	0.12	14.48	0.08	---	---	---	---	0.49
130	279.635	-33.6439	RPJ 051642-685541	T	15.55	0.03	14.83	0.03	14.68	0.05	---	---	14.56	0.07	14.28	0.16	---	---	0.86
131	278.734	-33.7794	RPJ 051652-681001	L	15.57	0.03	14.97	0.04	14.76	0.05	14.48	0.06	14.30	0.05	---	---	---	---	0.60
132	280.082	-33.5466	RPJ 051654-691845	T	---	---	---	---	---	---	15.74	0.10	---	---	---	---	---	---	1.54
134	279.448	-33.6218	RPJ 051717-684650	T	---	---	---	---	---	---	16.67	0.13	16.56	0.13	---	---	---	---	0.21
135	279.444	-33.6195	RPJ 051719-684640	P	15.34	0.03	14.83	0.03	14.51	0.04	14.26	0.05	14.20	0.06	14.19	0.14	---	---	0.61
136	281.673	-33.1812	RPJ 051746-704119	T	17.59	0.12	17.03	0.15	---	---	16.73	0.09	---	---	---	---	---	---	0.71
138	280.006	-33.4387	RPJ 051815-691621	P	---	---	---	---	---	---	15.55	0.08	15.15	0.07	13.23	0.09	11.54	0.07	0.58
141	277.253	-33.8409	RPJ 051837-665645	T	---	---	---	---	---	---	---	---	14.18	0.06	12.85	0.06	11.16	0.04	0.44
143	280.375	-33.3149	RPJ 051855-693559	T	---	---	---	---	---	---	15.73	0.07	15.52	0.10	---	---	---	---	0.70
144	281.382	-33.1298	RPJ 051900-702744	L	---	---	---	---	---	---	17.00	0.09	---	---	---	---	---	---	2.85
148	281.472	-33.0911	RPJ 051916-703237	T	17.35	0.09	16.96	0.13	16.63	0.23	16.40	0.06	16.01	0.08	---	---	---	---	0.36
153	281.583	-33.0139	RPJ 051956-703903	T	16.68	0.06	16.05	0.07	15.84	0.11	15.52	0.05	15.46	0.09	---	---	---	---	0.51

Table 3 (cont.)

#	/		b deg	NAME	STAT	J mag	σ_J mag	H mag	σ_H mag	K _S mag	σ_{K_S} mag	[3.6]		[4.5]		[5.8]		[8.0]		$\sigma_{8.0}$ mag	r arcs	
	deg	deg										mag	mag	mag	mag	mag	mag	mag	mag			mag
154	280.557	-33.1915	RPJ 051958-694623	T	---	---	---	---	---	15.00	0.07	13.64	0.05	13.06	0.05	12.56	0.10	12.02	0.08	0.55		
156	280.436	-33.1915	RPJ 052011-694028	T	10.58	0.03	9.64	0.03	9.08	0.03	8.17	0.05	8.02	0.04	7.76	0.03	7.53	0.03	7.53	0.03	1.76	
157	279.353	-33.3613	RPJ 052016-684510	L	15.38	0.04	14.67	0.04	14.54	0.04	14.13	0.06	14.18	0.07	14.11	0.15	---	---	---	---	0.09	
158	280.701	-33.1382	RPJ 052017-695407	T	---	---	---	---	---	---	16.53	0.12	16.48	0.11	---	---	---	---	---	---	1.44	
159	279.139	-33.39	RPJ 052020-683421	T	---	---	---	---	---	---	16.13	0.09	15.29	0.09	---	---	---	12.51	0.07	0.58	---	
160	279.153	-33.3651	RPJ 052034-683518	P	16.47	0.05	15.79	0.05	14.60	0.04	12.94	0.04	12.21	0.04	11.19	0.03	9.49	0.03	0.31	---	---	
161	279.422	-33.3213	RPJ 052035-684901	L	---	---	---	---	---	---	17.01	0.11	16.68	0.15	---	---	---	---	---	---	0.51	
163	281.052	-33.0313	RPJ 052049-701241	L	15.94	0.05	15.83	0.07	15.78	0.13	15.72	0.07	15.79	0.12	---	---	---	---	---	---	2.79	
164	280.609	-33.1025	RPJ 052052-695002	T	---	---	---	---	---	---	15.55	0.10	---	---	---	---	---	---	---	---	1.25	
166	280.589	-33.094	RPJ 052100-694907	T	14.99	0.03	14.28	0.03	14.16	0.03	14.07	0.06	14.07	0.07	13.83	0.13	---	---	---	---	1.68	
167	280.335	-33.1159	RPJ 052114-693621	T	---	---	---	---	---	---	---	---	16.45	0.16	---	---	---	---	---	---	0.91	
168	280.947	-33.0138	RPJ 052114-700745	T	---	---	---	---	---	---	16.85	0.13	16.52	0.13	---	---	---	---	---	---	1.57	
173	278.267	-33.4125	RPJ 052129-675106	T	13.00	0.03	12.02	0.03	10.46	0.03	7.99	0.04	6.97	0.04	5.89	0.04	4.15	0.04	0.33	---	---	
174	281.681	-32.8609	RPJ 052133-704548	T	13.34	0.03	12.44	0.03	12.18	0.03	11.97	0.05	12.14	0.04	11.94	0.07	11.85	0.08	2.56	---	---	
175	277.247	-33.5365	RPJ 052141-665931	T	---	---	---	---	---	---	14.54	0.06	13.60	0.05	12.62	0.07	11.08	0.03	0.73	---	---	
176	280.459	-33.0467	RPJ 052147-694315	T	15.82	0.05	15.69	0.08	15.51	0.09	15.14	0.12	14.96	0.09	---	---	---	---	---	---	0.60	
177	280.464	-33.0408	RPJ 052150-694334	P	---	---	---	---	---	---	16.29	0.12	---	---	---	---	---	---	---	---	1.09	
178	279.821	-33.1408	RPJ 052152-691043	T	---	---	---	---	---	---	14.52	0.05	13.77	0.07	13.05	0.06	12.27	0.05	0.27	---	---	
179	279.59	-33.1682	RPJ 052158-685859	T	14.63	0.03	13.77	0.03	13.62	0.03	13.54	0.04	13.62	0.05	13.67	0.11	---	---	---	---	1.77	
180	280.582	-32.9908	RPJ 052212-694957	P	13.44	0.02	13.13	0.03	13.10	0.03	13.02	0.07	13.06	0.05	12.99	0.16	---	---	---	---	1.14	
183	278.478	-33.3042	RPJ 052218-680239	T	16.23	0.05	15.74	0.06	15.27	0.08	14.51	0.14	---	---	---	---	---	---	---	---	0.37	
185	280.779	-32.9451	RPJ 052221-700013	T	14.51	0.03	13.73	0.03	13.55	0.03	13.45	0.06	13.46	0.06	13.48	0.08	---	---	---	---	2.42	
186	281.434	-32.8319	RPJ 052223-703355	T	14.99	0.03	14.39	0.03	14.38	0.05	14.36	0.13	14.17	0.12	14.09	0.16	---	---	---	---	1.05	
187	281.495	-32.818	RPJ 052226-703706	P	---	---	---	---	---	---	16.37	0.07	15.99	0.08	---	---	---	---	13.37	0.09	0.64	---
188	276.971	-33.4902	RPJ 052231-664621	L	---	---	---	---	---	---	---	---	14.49	0.08	---	---	---	---	---	---	1.44	---

Table 3 (cont.)

#	/		NAME	STAT	J	σ_J		H		σ_H		K _S		σ_{K_S}		[3.6]		$\sigma_{3.6}$		[4.5]		$\sigma_{4.5}$		[5.8]		$\sigma_{5.8}$		[8.0]		$\sigma_{8.0}$		r				
	deg	deg				mag	mag	mag	mag	mag	mag	mag	mag	mag	mag	mag	mag	mag	mag	mag	mag	mag	mag	mag	mag	mag	mag	mag	mag	mag	mag		mag	mag	mag	
190	278.324	-33.2939	RPJ 052238-675508	T	15.05	0.03	14.87	0.04	14.75	0.06	14.49	0.09	14.33	0.14	---	---	---	---	---	---	---	---	---	---	---	---	---	---	---	---	---	---	---	0.26		
191	280.347	-32.9817	RPJ 052243-693828	T	12.60	0.03	11.33	0.03	10.20	0.02	8.81	0.05	8.16	0.03	7.55	0.03	7.55	0.03	7.55	0.03	7.55	0.03	7.55	0.03	7.55	0.03	6.96	0.02	0.29	---	---	---	---	0.85		
192	276.859	-33.4751	RPJ 052249-664055	P	14.74	0.03	14.11	0.04	13.23	0.04	---	---	---	---	---	---	---	---	---	---	---	---	---	---	---	---	---	---	---	---	---	---	---	---	0.25	
193	279.163	-33.1504	RPJ 052252-683805	T	---	---	---	---	---	---	17.28	0.13	---	---	---	---	---	---	---	---	---	---	---	---	---	---	---	---	---	---	---	---	---	0.25		
194	280.385	-32.9605	RPJ 052254-694036	L	13.17	0.02	13.08	0.04	13.02	0.04	12.89	0.05	12.84	0.05	12.90	0.10	12.90	0.10	12.71	0.10	12.71	0.10	12.71	0.10	12.71	0.10	12.71	0.10	1.53	---	---	---	---	2.17		
195	280.371	-32.9438	RPJ 052307-694004	T	---	---	---	---	---	---	15.76	0.09	15.77	0.16	---	---	---	---	---	---	---	---	---	---	---	---	---	---	---	---	---	---	---	0.20		
196	280.553	-32.9086	RPJ 052311-694929	T	---	---	---	---	---	---	15.27	0.12	15.48	0.14	---	---	---	---	---	---	---	---	---	---	---	---	---	---	---	---	---	---	---	1.28		
197	281.01	-32.8201	RPJ 052321-701305	T	16.37	0.08	15.81	0.08	15.60	0.11	15.56	0.08	15.63	0.11	---	---	---	---	---	---	---	---	---	---	---	---	---	---	---	---	---	---	---	0.94		
198	280.722	-32.8504	RPJ 052332-695831	P	12.07	0.03	11.17	0.03	10.78	0.02	10.44	0.04	10.68	0.03	10.46	0.03	10.46	0.03	10.39	0.04	10.39	0.04	10.39	0.04	10.39	0.04	10.39	0.04	0.94	---	---	---	---	1.77		
199	280.026	-32.9294	RPJ 052352-692309	T	16.47	0.08	15.93	0.09	---	---	15.51	0.09	15.56	0.10	---	---	---	---	---	---	---	---	---	---	---	---	---	---	---	---	---	---	---	---	0.97	
203	279.955	-32.9148	RPJ 052409-691947	T	12.63	0.02	11.59	0.03	11.18	0.03	10.90	0.04	10.88	0.03	10.67	0.04	10.67	0.04	10.38	0.07	10.38	0.07	10.38	0.07	10.38	0.07	10.38	0.07	0.97	---	---	---	---	0.58		
209	277.312	-33.2654	RPJ 052421-670516	T	---	---	---	---	---	---	16.31	0.08	16.15	0.10	---	---	---	---	---	---	---	---	---	---	---	---	---	---	---	---	---	---	---	---	0.25	
211	279.563	-32.9385	RPJ 052432-690006	L	15.01	0.04	14.44	0.04	14.19	0.04	13.77	0.08	13.82	0.08	13.72	0.13	---	---	---	---	---	---	---	---	---	---	---	---	---	---	---	---	---	0.19		
212	279.642	-32.9179	RPJ 052438-690413	T	15.30	0.04	15.01	0.05	14.86	0.06	14.82	0.11	14.76	0.06	---	---	---	---	---	---	---	---	---	---	---	---	---	---	---	---	---	---	---	1.41		
213	280.933	-32.7058	RPJ 052449-701034	T	---	---	---	---	---	---	15.93	0.15	15.93	0.15	---	---	---	---	---	---	---	---	---	---	---	---	---	---	---	---	---	---	---	---	0.26	
214	279.613	-32.8923	RPJ 052458-690304	P	15.17	0.03	15.08	0.05	14.85	0.06	14.32	0.06	14.15	0.05	13.88	0.14	---	---	---	---	---	---	---	---	---	---	---	---	---	---	---	---	---	---	1.29	
216	280.5	-32.7519	RPJ 052504-694833	T	---	---	---	---	---	---	15.41	0.11	15.55	0.09	---	---	---	---	---	---	---	---	---	---	---	---	---	---	---	---	---	---	---	---	0.54	
217	280.521	-32.734	RPJ 052514-694949	T	15.65	0.04	15.02	0.06	14.94	0.07	14.64	0.08	14.89	0.10	---	---	---	---	---	---	---	---	---	---	---	---	---	---	---	---	---	---	---	---	1.98	
218	279.301	-32.8717	RPJ 052541-684746	T	---	---	---	---	---	---	---	---	16.35	0.15	---	---	---	---	---	---	---	---	---	---	---	---	---	---	---	---	---	---	---	---	0.96	
219	277.657	-33.0639	RPJ 052558-672413	T	13.79	0.02	13.85	0.03	13.92	0.03	13.83	0.04	13.90	0.06	13.82	0.10	---	---	---	---	---	---	---	---	---	---	---	---	---	---	---	---	---	---	0.06	
220	281.016	-32.5762	RPJ 052611-701605	T	---	---	---	---	---	---	15.59	0.06	15.16	0.08	---	---	---	---	---	---	---	---	---	---	---	---	---	---	---	---	---	---	---	---	1.81	
221	281.848	-32.4436	RPJ 052612-705855	T	---	---	---	---	---	---	16.26	0.09	16.09	0.13	---	---	---	---	---	---	---	---	---	---	---	---	---	---	---	---	---	---	---	---	0.41	
222	280.034	-32.7186	RPJ 052613-692545	L	---	---	---	---	---	---	17.27	0.12	17.33	0.17	---	---	---	---	---	---	---	---	---	---	---	---	---	---	---	---	---	---	---	---	0.46	
224	280.852	-32.5799	RPJ 052625-700754	T	---	---	---	---	---	---	15.21	0.08	12.59	0.05	11.68	0.03	10.95	0.04	10.06	0.03	10.06	0.03	10.06	0.03	10.06	0.03	10.06	0.03	0.46	---	---	---	---	1.77		
225	280.855	-32.5789	RPJ 052626-700805	T	---	---	---	---	---	---	16.29	0.12	---	---	---	---	---	---	---	---	---	---	---	---	---	---	---	---	---	---	---	---	---	---	---	---

Table 3 (cont.)

#	l		b deg	NAME	STAT	J mag	σ_J mag	H mag	σ_H mag	K _S mag	σ_{K_S} mag	[3.6]		[4.5]		[5.8]		[8.0]		$\sigma_{8.0}$ mag	r arcs
	deg	deg										mag	mag	mag	mag	mag	mag	mag	mag		
228	281.261	-32.501	RPJ 052637-702907	T	---	---	---	---	---	---	---	13.53	0.05	12.58	0.03	11.73	0.04	10.70	0.03	1.28	---
229	281.87	-32.4037	RPJ 052639-710027	T	16.55	0.08	16.14	0.11	---	---	---	15.85	0.09	15.75	0.14	---	---	---	---	---	2.82
230	278.055	-32.9426	RPJ 052642-674505	P	---	---	---	---	---	---	---	15.49	0.08	15.00	0.10	---	---	---	---	---	0.46
232	278.068	-32.928	RPJ 052650-674554	P	17.16	0.08	16.49	0.12	15.73	0.11	13.65	0.04	12.87	0.04	12.02	0.06	11.11	0.07	0.90	---	---
233	279.77	-32.689	RPJ 052658-69125	L	16.24	0.06	15.69	0.07	15.51	0.10	15.33	0.08	15.35	0.11	---	---	---	---	---	---	0.11
234	281.198	-32.4633	RPJ 052711-702623	T	---	---	---	---	---	---	---	16.97	0.09	---	---	---	---	---	---	---	1.94
236	280.733	-32.5181	RPJ 052721-700235	T	---	---	---	---	---	---	---	---	---	16.16	0.11	---	---	---	---	---	1.02
237	278.743	-32.782	RPJ 052728-682052	L	15.79	0.04	15.15	0.05	15.06	0.07	14.56	0.05	14.48	0.07	---	---	---	---	---	---	1.21
242	279.495	-32.627	RPJ 052804-685947	L	15.75	0.05	14.77	0.06	13.47	0.03	11.06	0.08	10.12	0.05	9.29	0.11	---	---	---	---	0.59
244	280.484	-32.4842	RPJ 052809-695032	T	---	---	---	---	---	---	---	16.20	0.08	16.41	0.14	---	---	---	---	---	0.95
245	277.332	-32.8847	RPJ 052812-670935	T	16.23	0.05	15.64	0.06	15.53	0.10	15.54	0.08	15.56	0.11	---	---	---	---	---	---	2.80
247	280.433	-32.4601	RPJ 052830-694814	T	---	---	---	---	---	---	---	15.82	0.11	15.67	0.11	---	---	---	---	---	1.63
249	280.549	-32.4244	RPJ 052844-695422	T	14.24	0.03	13.43	0.04	13.30	0.04	13.07	0.04	13.19	0.04	13.19	0.09	13.02	0.09	0.39	---	---
250	277.03	-32.8622	RPJ 052846-665440	T	15.59	0.03	14.91	0.04	14.75	0.06	14.69	0.05	14.63	0.07	14.51	0.15	---	---	---	---	1.01
251	279.561	-32.537	RPJ 052858-690354	P	---	---	16.29	0.12	---	---	---	16.02	0.11	15.60	0.13	---	---	---	---	---	0.67
252	280.399	-32.4148	RPJ 052905-694657	T	16.07	0.06	15.59	0.07	15.44	0.10	15.26	0.06	15.18	0.06	---	---	---	---	---	---	0.88
253	280.348	-32.409	RPJ 052913-694428	T	---	---	---	---	---	---	---	15.50	0.08	14.66	0.07	13.43	0.11	11.87	0.06	1.50	---
255	279.524	-32.5073	RPJ 052921-690220	P	14.58	0.03	13.75	0.03	13.58	0.03	13.50	0.06	13.58	0.06	13.41	0.12	---	---	---	---	2.00
257	280.363	-32.3777	RPJ 052933-694531	T	---	---	---	---	---	---	---	15.97	0.08	16.04	0.11	---	---	---	---	---	0.41
260	276.756	-32.7942	RPJ 052946-664130	T	16.95	0.07	16.59	0.12	16.42	0.21	16.43	0.10	16.40	0.11	---	---	---	---	---	---	2.92
262	276.756	-32.7923	RPJ 052947-664130	L	16.52	0.05	15.97	0.07	15.66	0.12	15.71	0.07	15.67	0.09	---	---	---	---	---	---	2.31
265	280.143	-32.3553	RPJ 053009-693445	P	14.26	0.03	13.48	0.03	13.33	0.03	13.27	0.05	13.29	0.05	13.21	0.06	13.13	0.08	0.73	---	---
267	279.481	-32.4352	RPJ 053013-690050	T	---	---	---	---	---	---	---	16.92	0.10	16.20	0.13	---	---	---	---	---	0.18
269	280.923	-32.2255	RPJ 053026-701501	P	---	---	---	---	---	---	---	16.68	0.13	---	---	---	---	---	---	---	2.89
270	277.063	-32.684	RPJ 053033-665741	L	---	---	---	---	---	---	---	16.16	0.07	15.76	0.11	---	---	---	---	---	0.57

Table 3 (cont.)

#	l		b		NAME	STAT	J	σ_J		H	σ_H		K _s	σ_{Ks}		[3.6]	$\sigma_{3.6}$		[4.5]	$\sigma_{4.5}$		[5.8]	$\sigma_{5.8}$		[8.0]	$\sigma_{8.0}$		r
	deg	deg	mag	mag				mag	mag		mag	mag		mag	mag		mag	mag		mag	mag		mag	mag		mag	mag	
271	280.923	-32.2015	RPJ 053043-701515	T	---	---	---	---	---	---	---	---	---	---	---	15.64	0.08	15.43	0.10	---	---	---	---	---	---	---	---	1.33
272	279.044	-32.4423	RPJ 053044-683853	T	---	---	---	---	---	---	---	---	---	---	---	17.56	0.13	---	---	---	---	---	---	---	---	---	---	0.56
274	277.498	-32.6013	RPJ 053055-672005	P	15.25	0.07	14.22	0.06	12.98	0.04	10.81	0.05	9.98	0.04	8.79	0.05	9.98	0.04	8.79	0.05	7.40	0.05	1.31	---	---	---	---	
275	280.409	-32.2498	RPJ 053057-694900	T	---	---	---	---	---	---	15.40	0.05	15.51	0.06	---	---	---	---	---	---	---	---	---	---	---	---	0.12	
276	278.978	-32.4263	RPJ 053059-683542	T	16.04	0.05	15.02	0.05	13.76	0.04	---	---	---	---	---	---	---	---	11.65	0.09	10.30	0.05	8.57	0.05	0.96	---	---	
277	279.66	-32.3327	RPJ 053106-691042	P	---	---	---	---	---	---	14.87	0.12	14.81	0.13	---	---	---	---	---	---	---	---	---	---	---	---	0.44	
278	278.818	-32.4238	RPJ 053113-682742	P	17.30	0.11	16.69	0.15	15.90	0.15	14.42	0.05	13.83	0.06	13.43	0.09	12.87	0.10	0.58	---	---	---	---	---	---	---	---	
279	281.673	-32.0461	RPJ 053119-705422	L	15.65	0.03	15.11	0.05	14.84	0.06	14.51	0.06	14.44	0.05	14.20	0.13	---	---	---	---	---	---	---	---	---	---	0.97	
280	278.891	-32.4037	RPJ 053120-683134	P	---	---	---	---	---	---	16.25	0.07	16.30	0.13	---	---	---	---	---	---	---	---	---	---	---	---	0.42	
281	280.433	-32.1999	RPJ 053129-695042	T	---	---	---	---	---	---	17.14	0.13	---	---	---	---	---	---	---	---	---	---	---	---	---	---	0.38	
283	282.043	-31.9632	RPJ 053141-711346	L	14.81	0.03	14.24	0.03	13.97	0.03	13.66	0.05	13.60	0.04	13.59	0.11	---	---	---	---	---	---	---	---	---	---	0.53	
286	281.972	-31.969	RPJ 053145-711008	P	---	---	---	---	---	---	16.80	0.09	16.44	0.13	---	---	---	---	---	---	---	---	---	---	---	---	0.07	
287	280.331	-32.1874	RPJ 053147-694541	T	---	---	---	---	---	---	16.65	0.10	16.52	0.14	---	---	---	---	---	---	---	---	---	---	---	---	0.45	
290	281.967	-31.9624	RPJ 053150-710955	P	16.14	0.05	15.43	0.06	15.25	0.08	14.92	0.06	14.80	0.06	---	---	---	---	---	---	---	---	---	---	---	---	1.35	
292	281.515	-32.0149	RPJ 053157-704646	T	---	---	---	---	---	---	17.08	0.15	---	---	---	---	---	---	---	---	---	---	---	---	---	---	0.24	
293	279.032	-32.3081	RPJ 053212-683924	P	14.82	0.02	14.21	0.03	13.96	0.03	13.63	0.04	13.57	0.04	13.53	0.10	---	---	---	---	---	---	---	---	---	---	0.12	
294	281.521	-31.9718	RPJ 053228-704728	P	15.36	0.03	14.73	0.04	14.48	0.05	14.25	0.06	14.20	0.06	14.09	0.14	---	---	---	---	---	---	---	---	---	---	0.79	
297	279.915	-32.1712	RPJ 053233-692456	L	---	---	---	---	---	---	16.16	0.09	15.89	0.11	---	---	---	---	---	---	---	---	---	---	---	---	0.27	
299	280.049	-32.1466	RPJ 053239-693152	T	---	---	---	---	14.78	0.05	12.41	0.06	11.60	0.03	10.63	0.05	9.15	0.05	0.99	---	---	---	---	---	---	---	---	
300	280.028	-32.1484	RPJ 053239-693049	T	16.97	0.12	16.04	0.10	14.93	0.07	12.13	0.08	11.31	0.05	10.29	0.07	8.87	0.06	0.03	---	---	---	---	---	---	---	---	
302	281.347	-31.9752	RPJ 053242-703840	T	---	---	---	---	---	---	16.15	0.09	16.29	0.14	---	---	---	---	---	---	---	---	---	---	---	---	1.75	
304	281.318	-31.9671	RPJ 053251-703717	T	---	---	---	---	---	---	16.55	0.10	---	---	---	---	---	---	---	---	---	---	---	---	---	---	0.25	
305	277.883	-32.3727	RPJ 053252-674108	P	15.42	0.04	14.47	0.04	13.25	0.03	10.87	0.07	10.07	0.04	8.75	0.05	7.19	0.06	0.36	---	---	---	---	---	---	---	---	
306	280.974	-32.0108	RPJ 053252-701935	T	---	---	---	---	---	---	16.62	0.12	---	---	---	---	---	---	---	---	---	---	---	---	---	---	1.69	
310	282.104	-31.8368	RPJ 053308-711803	T	---	---	---	---	---	---	14.90	0.06	14.23	0.07	13.52	0.11	11.79	0.07	0.06	---	---	---	---	---	---	---	---	

Table 3 (cont.)

#	<i>l</i> deg	<i>b</i> deg	NAME	STAT	J mag	σ_J mag	H mag	σ_H mag	K _S mag	σ_{K_S} mag	[3.6] mag	$\sigma_{3.6}$ mag	[4.5] mag	$\sigma_{4.5}$ mag	[5.8] mag	$\sigma_{5.8}$ mag	[8.0] mag	$\sigma_{8.0}$ mag	<i>r</i> arcs
311	279.018	-32.2016	RPJ 053323-683933	L	---	---	---	---	---	---	16.49	0.11	16.17	0.12	---	---	---	---	0.19
315	277.555	-32.3406	RPJ 053333-672454	L	14.48	0.03	14.61	0.03	14.58	0.05	14.63	0.04	14.67	0.05	14.59	0.15	---	---	0.13
316	279.663	-32.1022	RPJ 053340-691250	P	15.45	0.03	15.07	0.05	14.79	0.05	14.29	0.05	14.09	0.05	14.03	0.14	---	---	0.69
317	279.915	-31.9822	RPJ 053441-692630	T	12.47	0.02	10.99	0.02	9.91	0.03	8.95	0.05	8.25	0.03	7.75	0.03	7.25	0.02	0.51
318	279.175	-32.0551	RPJ 053448-684835	T	---	---	---	---	---	---	15.14	0.07	14.45	0.06	13.14	0.09	11.24	0.05	0.50
320	280.544	-31.8445	RPJ 053525-695921	T	13.94	0.03	13.07	0.03	12.82	0.03	12.73	0.03	12.83	0.04	12.78	0.07	12.55	0.06	0.78
321	277.789	-32.1302	RPJ 053530-673805	P	17.00	0.08	16.64	0.14	---	---	16.55	0.15	---	---	---	---	---	---	0.48
322	276.871	-32.1907	RPJ 053544-665122	P	16.58	0.06	16.00	0.08	15.79	0.12	15.43	0.06	15.30	0.07	---	---	---	---	0.91
324	277.021	-32.1682	RPJ 053549-665905	T	---	---	---	---	---	---	17.39	0.12	---	---	---	---	---	---	0.44
325	279.397	-31.9272	RPJ 053556-690045	P	---	---	---	---	12.63	0.05	10.16	0.03	9.20	0.03	8.42	0.03	7.43	0.03	0.27
326	277.922	-32.0663	RPJ 053602-674516	P	16.88	0.07	15.81	0.07	14.60	0.05	12.87	0.04	12.17	0.04	11.41	0.05	10.29	0.05	0.79
327	282.045	-31.5976	RPJ 053611-711719	T	---	---	---	---	---	---	16.85	0.17	---	---	---	---	---	---	2.57
328	282.047	-31.5958	RPJ 053612-711724	P	14.11	0.02	13.79	0.03	13.80	0.03	13.76	0.06	13.68	0.07	13.67	0.16	---	---	2.98
329	279.309	-31.9094	RPJ 053614-685627	P	---	---	---	---	16.01	0.15	15.27	0.11	15.02	0.08	---	---	---	---	2.87
331	281.113	-31.6823	RPJ 053632-702925	T	16.69	0.08	16.00	0.10	---	---	15.82	0.07	15.96	0.10	---	---	---	---	2.75
332	279.811	-31.8257	RPJ 053635-692228	L	---	---	---	---	---	---	16.79	0.14	16.43	0.14	---	---	---	---	0.66
334	281.027	-31.6847	RPJ 053638-702505	T	---	---	---	---	---	---	---	---	16.91	0.14	---	---	---	---	0.82
335	279.803	-31.8177	RPJ 053641-692208	P	16.53	0.06	15.97	0.08	16.05	0.15	15.65	0.07	15.66	0.13	---	---	---	---	0.76
336	277.674	-32.0221	RPJ 053644-673259	P	15.55	0.04	15.00	0.04	14.92	0.06	14.51	0.05	14.46	0.05	---	---	---	---	0.41
337	279.891	-31.7972	RPJ 053648-692644	P	---	---	---	---	---	---	16.04	0.07	15.77	0.09	---	---	---	---	0.27
338	279.836	-31.802	RPJ 053649-692355	L	16.56	0.06	16.21	0.10	---	---	15.45	0.09	15.28	0.13	---	---	---	---	0.86
339	277.69	-32.0014	RPJ 053656-673356	P	16.82	0.08	16.13	0.11	15.69	0.13	---	---	---	---	12.08	0.17	---	---	0.71
340	279.786	-31.7905	RPJ 053700-692128	T	16.69	0.07	16.26	0.10	16.00	0.15	15.92	0.09	15.76	0.07	---	---	---	---	1.31
342	278.484	-31.9155	RPJ 053704-681442	P	17.01	0.09	16.06	0.10	15.27	0.09	---	---	12.88	0.14	10.86	0.16	---	---	1.17

Table 3 (cont.)

#	/		NAME	STAT	J	σ_J	H	σ_H	K _S	σ_{K_S}	[3.6]		[4.5]		[5.8]		[8.0]		$\sigma_{8.0}$	r
	deg	deg									mag	mag	mag	mag	mag	mag	mag	mag		
344	279.895	-31.7702	RPJ 053706-692709	P	---	---	---	---	---	---	16.02	0.10	15.84	0.09	---	---	---	---	---	0.60
345	280.919	-31.6556	RPJ 053707-701951	T	---	---	---	---	---	---	17.11	0.13	---	---	---	---	---	---	---	0.82
346	282.146	-31.5057	RPJ 053710-712313	T	17.58	0.15	16.58	0.15	15.43	0.10	13.77	0.04	13.00	0.04	12.35	0.06	11.35	0.04	0.74	0.74
347	277.285	-32.0139	RPJ 053710-671323	L	16.01	0.04	15.20	0.05	15.09	0.07	14.90	0.07	14.87	0.05	---	---	---	---	---	0.25
355	280.681	-31.6518	RPJ 053729-700750	T	---	---	---	---	---	---	16.31	0.10	16.74	0.14	---	---	---	---	---	0.44
356	280.85	-31.6327	RPJ 053729-701633	T	---	---	---	---	---	---	12.94	0.06	12.96	0.03	12.72	0.09	12.65	0.08	0.50	0.50
357	281.901	-31.5066	RPJ 053731-711048	P	13.36	0.03	12.48	0.03	12.17	0.03	12.03	0.05	12.13	0.03	12.03	0.06	11.97	0.05	1.49	1.49
358	277.249	-31.9601	RPJ 053745-671153	T	15.17	0.03	14.61	0.03	14.29	0.04	13.83	0.05	13.82	0.05	13.80	0.13	---	---	---	0.44
359	279.979	-31.7025	RPJ 053746-693153	P	13.33	0.03	12.38	0.03	12.16	0.03	12.00	0.06	12.16	0.04	12.04	0.06	11.94	0.06	1.76	1.76
360	278.967	-31.8019	RPJ 053748-683954	P	16.59	0.07	16.51	0.14	16.22	0.19	15.45	0.07	15.20	0.10	---	---	---	---	0.22	0.22
361	281.156	-31.5403	RPJ 053810-703245	L	---	---	---	---	---	---	16.86	0.13	16.59	0.14	---	---	---	---	---	2.24
364	279.99	-31.6425	RPJ 053826-693251	P	14.51	0.03	14.15	0.03	14.07	0.04	13.93	0.05	13.91	0.06	---	---	---	---	2.62	2.62
367	280.883	-31.5279	RPJ 053840-701901	T	17.02	0.09	16.20	0.10	---	---	15.96	0.08	15.93	0.11	---	---	---	---	1.58	1.58
368	280.01	-31.6091	RPJ 053848-693407	P	---	---	---	---	---	---	15.85	0.07	15.49	0.13	---	---	---	---	0.49	0.49
372	280.027	-31.5861	RPJ 053902-693509	P	16.70	0.07	16.08	0.08	15.96	0.14	15.92	0.12	15.61	0.12	---	---	---	---	2.74	2.74
373	280.33	-31.5518	RPJ 053905-695045	L	---	---	---	---	---	---	16.11	0.10	16.08	0.16	---	---	---	---	2.46	2.46
375	280.028	-31.5794	RPJ 053907-693514	P	15.59	0.04	15.55	0.06	15.24	0.08	15.33	0.12	---	---	---	---	---	---	0.24	0.24
376	278.863	-31.6769	RPJ 053916-683527	T	17.21	0.10	16.34	0.12	15.27	0.08	13.99	0.05	13.43	0.04	12.92	0.07	12.12	0.05	0.56	0.56
377	281.114	-31.4442	RPJ 053922-703124	T	---	---	---	---	---	---	16.77	0.11	16.18	0.11	---	---	---	---	1.45	1.45
378	279.318	-31.6143	RPJ 053930-685857	P	---	---	---	---	---	---	15.77	0.10	15.44	0.11	---	---	---	---	0.22	0.22
382	281.872	-31.3325	RPJ 053942-711044	P	---	---	---	---	14.95	0.07	11.95	0.06	11.07	0.05	10.09	0.04	8.88	0.03	0.95	0.95
384	281.837	-31.3234	RPJ 053952-710902	T	17.14	0.10	16.15	0.10	15.30	0.09	12.82	0.08	12.11	0.04	10.06	0.03	8.48	0.02	0.66	0.66
387	279.3	-31.5581	RPJ 054008-685826	P	16.25	0.05	16.07	0.09	15.94	0.16	15.12	0.07	14.64	0.08	13.96	0.13	---	---	0.52	0.52
388	278.732	-31.5918	RPJ 054019-682919	P	---	---	---	---	---	---	16.61	0.06	16.31	0.07	---	---	---	---	0.46	0.46
389	279.582	-31.5142	RPJ 054020-691300	P	---	---	---	---	---	---	15.40	0.07	15.31	0.07	---	---	---	---	0.76	0.76

Table 3 (cont.)

#	/	b	NAME	STAT J	σ_J	H	σ_H	K _S	σ_{K_S}	[3.6]	$\sigma_{3.6}$	[4.5]	$\sigma_{4.5}$	[5.8]	$\sigma_{5.8}$	[8.0]	$\sigma_{8.0}$	r	
deg	deg	deg		mag	mag	mag	mag	mag	mag	mag	mag	mag	mag	mag	mag	mag	mag	mag	arcs
390	281.58	-31.3027	RPJ 054028-705609 P	15.73	0.04	15.12	0.05	14.99	0.06	14.89	0.06	15.04	0.08	---	---	---	---	2.78	
391	280.389	-31.4255	RPJ 054028-695439 T	---	---	---	---	---	---	16.33	0.10	16.02	0.12	---	---	---	---	0.43	
392	281.125	-31.3436	RPJ 054033-703240 L	---	---	---	---	---	---	12.97	0.04	12.13	0.02	10.72	0.03	8.90	0.02	0.51	
394	281.034	-31.3366	RPJ 054045-702806 T	15.11	0.03	14.49	0.04	13.53	0.04	11.00	0.05	10.05	0.05	8.88	0.05	---	---	0.96	
395	281.362	-31.291	RPJ 054053-704508 T	---	---	16.71	0.14	---	---	16.43	0.11	16.30	0.14	---	---	---	---	2.86	
396	278.931	-31.5204	RPJ 054055-683954 P	---	---	---	---	---	---	16.97	0.14	16.25	0.09	---	---	---	---	0.50	
397	279.597	-31.4611	RPJ 054055-691409 P	---	---	---	---	---	---	15.55	0.08	15.33	0.09	---	---	---	---	0.58	
401	281.654	-31.2181	RPJ 054124-710030 P	---	---	---	---	---	---	16.73	0.09	---	---	---	---	---	---	1.71	
403	279.084	-31.4595	RPJ 054126-684802 P	14.97	0.03	14.38	0.03	14.11	0.03	13.73	0.07	13.64	0.04	13.67	0.11	---	---	1.38	
405	281.025	-31.2426	RPJ 054152-702818 T	16.40	0.07	15.72	0.08	15.47	0.09	15.48	0.07	15.24	0.16	---	---	---	---	2.65	
406	281.72	-31.1706	RPJ 054153-710415 T	15.09	0.03	14.46	0.03	14.33	0.04	14.21	0.05	14.29	0.04	14.21	0.15	---	---	2.94	
407	280.959	-31.2361	RPJ 054202-702459 T	---	---	---	---	---	---	17.58	0.16	---	---	---	---	---	---	0.79	
414	281.03	-31.1811	RPJ 054236-702859 T	---	---	---	---	---	---	17.13	0.14	---	---	---	---	---	---	2.06	
416	281.113	-31.1372	RPJ 054302-703332 T	16.63	0.07	16.08	0.10	15.79	0.13	15.86	0.06	15.85	0.10	---	---	---	---	2.93	
417	277.955	-31.3836	RPJ 054312-675053 P	15.92	0.04	15.96	0.09	---	---	16.08	0.07	15.96	0.09	---	---	---	---	0.28	
418	280.4	-31.1811	RPJ 054317-695651 T	---	---	---	---	---	---	15.72	0.16	---	---	---	---	---	---	0.42	
420	279.776	-31.2165	RPJ 054330-692446 P	16.14	0.11	14.78	0.10	12.71	0.03	9.94	0.03	8.79	0.05	7.81	0.03	6.46	0.03	0.17	
422	281.116	-31.0858	RPJ 054338-703401 P	---	---	---	---	---	---	16.28	0.11	---	---	---	---	---	---	0.16	
425	279.625	-31.1616	RPJ 054415-691722 P	16.72	0.06	16.48	0.11	---	---	16.01	0.14	---	---	---	---	---	---	0.39	
429	279.611	-31.1486	RPJ 054425-691642 P	15.43	0.03	15.16	0.04	14.96	0.06	14.33	0.06	14.05	0.06	---	---	---	---	0.15	
433	280.039	-31.081	RPJ 054448-693859 P	16.22	0.05	15.93	0.08	15.86	0.13	15.75	0.11	15.64	0.08	---	---	---	---	0.24	
434	279.637	-31.0951	RPJ 054500-691819 P	17.39	0.12	15.72	0.07	13.70	0.03	10.72	0.03	9.67	0.03	8.82	0.04	7.86	0.03	0.33	
435	277.544	-31.237	RPJ 054501-673034 T	---	---	---	---	---	---	17.39	0.14	---	---	---	---	---	---	2.73	

Table 3 (cont.)

#	l deg	b deg	NAME	STAT	J mag	σ_J mag	H mag	σ_H mag	Ks mag	σ_{Ks} mag	[3.6] mag	$\sigma_{3.6}$ mag	[4.5] mag	$\sigma_{4.5}$ mag	[5.8] mag	$\sigma_{5.8}$ mag	[8.0] mag	$\sigma_{8.0}$ mag	r arcs
436	279.478	-31.0911	RPJ 054511-691013	P	---	---	---	---	---	---	16.07	0.05	15.76	0.07	---	---	---	---	0.23
437	281.585	-30.9131	RPJ 054512-705905	T	---	---	---	---	---	---	16.93	0.13	---	---	---	---	---	---	2.06
438	280.028	-31.0428	RPJ 054515-693837	P	---	---	---	---	---	---	16.81	0.13	---	---	---	---	---	---	1.21
439	280.186	-31.0289	RPJ 054515-694648	L	13.13	0.03	11.76	0.03	10.73	0.02	9.03	0.04	8.50	0.03	8.09	0.02	7.78	0.02	0.35
441	281.272	-30.9115	RPJ 054534-704303	T	---	---	---	---	---	---	16.39	0.10	16.23	0.13	---	---	---	---	2.47
443	279.447	-31.0233	RPJ 054558-690857	P	14.76	0.03	14.42	0.03	14.22	0.04	13.83	0.08	13.69	0.05	13.41	0.10	---	---	0.60
446	279.958	-30.9518	RPJ 054621-693531	T	---	---	---	---	---	---	16.48	0.09	---	---	---	---	---	---	2.41
447	280.932	-30.8711	RPJ 054623-702555	T	---	---	---	---	---	---	16.40	0.10	16.29	0.14	---	---	---	---	0.11
449	281.527	-30.7996	RPJ 054639-705650	T	---	---	---	---	---	---	16.13	0.14	15.94	0.15	14.06	0.12	12.64	0.06	0.67
451	280.98	-30.8145	RPJ 054701-702842	T	---	---	---	---	---	---	16.98	0.16	16.39	0.15	---	---	---	---	2.60
452	280.813	-30.7897	RPJ 054728-702015	T	---	---	---	---	---	---	16.69	0.09	16.25	0.11	---	---	---	---	1.61
454	278.07	-30.8898	RPJ 054822-675853	P	14.57	0.03	13.09	0.04	11.73	0.02	10.20	0.04	9.45	0.03	8.80	0.03	8.02	0.03	0.25
456	280.95	-30.6225	RPJ 054920-702809	T	16.16	0.04	15.69	0.06	15.62	0.12	15.35	0.07	15.42	0.08	---	---	---	---	1.47
458	280.574	-30.6029	RPJ 054953-700855	T	---	---	---	---	---	---	16.95	0.14	16.69	0.14	---	---	---	---	0.64

Figure Captions

Figure 1

The distributions of LMC nebulae (small blue disks) and Galactic bulge sources (large red disks) in the $[3.6]/([3.6]-[8.0])$ magnitude-colour plane, where the magnitudes of LMC sources have been reduced to the value they would have in the Galactic centre. The dashed lines indicate the SAGE completeness limits for the LMC nebulae. As would be expected, there are relatively few LMC nebulae below the two dashed completeness limits, in a region where most of the GBPNe appear to be located. This suggests that most of the LMC PNe have yet to be detected.

Figure 2

As for Fig. 1, but for the $[8.0]/([3.6]-[8.0])$ plane.

Figure 3

The variation in normalised source numbers with 3.6 and 8.0 μm magnitudes. Notice how the 3.6 μm bulge and LMC trends are closely similar, whilst the trends at 8.0 μm are well separated. This latter difference is attributed to incompleteness in the LMC 8.0 μm sample.

Figure 4

A comparison of 4.5 and 3.6 μm magnitudes (filled diamonds), and 8.0 and 3.6 μm magnitudes (open squares) for GBPNe (upper panel) and LMC PNe (lower panel). The sample is much greater in the lower panel, where it appears that there is little evolution of $[3.6]-[8.0]$ colour indices with 3.6 μm magnitude, and a strict upper limit of $[3.6]-[8.0] \cong 3.8$ mag upon the colours of the sources. The $[4.5]-[3.6]$ trend is close to that expected for bremsstrahlung and central star emission, and this leads to two closely parallel (and overlapping) sequences of points – those corresponding to nebulae in which bremsstrahlung and line emission is dominant (upper points), and those in which stellar emission is important.

Figure 5

Distribution of differing populations of planetary nebulae within the [3.6]-[4.5]/[4.5]-[8.0] colour plane, where the large red disks correspond to the Galactic bulge sources; diamonds to the Acker et al. (1992) Galactic disk sources; squares to the MASH GDPNe of Parker et al. (2006) and Miszalski et al. (2008); and the small blue disks to the LMC PNe – the latter results deriving from data presented in this paper, and photometry published by Hora et al. (2008). It will be noted that the differing categories of sources are similarity scattered throughout this plane.

Figure 6

As for Fig. 5, but for the [3.6]-[4.5]/[5.8]-[8.0] (top panel) and [5.8]-[8.0]/[4.5]-[5.8] (bottom panel) colour planes. Note the sharp cut-off in LMC PNe above [5.8]-[8.0] \sim 2 mag (top panel), and how the LMC sources are largely confined to the lower right-hand side of the [5.8]-[8.0]/[4.5]-[5.8] plane (bottom panel).

Figure 7

Distribution of differing categories of source with respect to the [3.6]-[4.5] colour index. The lower curve represents the trend for sources in which there are no detections at 5.8 or 8.0 μ m.

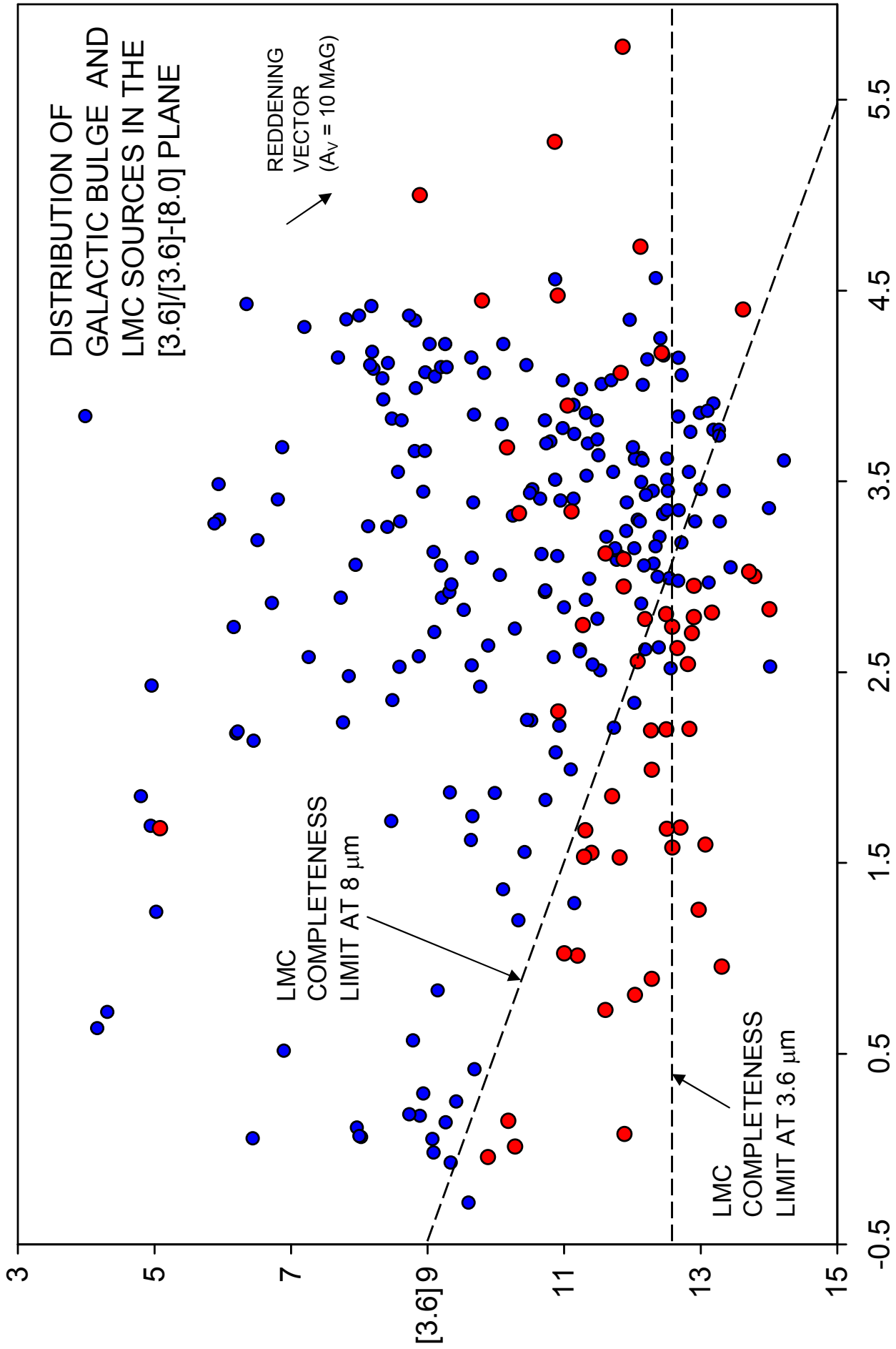
Figure 8

As for Fig. 7, but for the [4.5]-[8.0] (left panel) and [5.8]-[8.0] (right panel) colour indices. All of these sources are detected in the four IRAC bands.

Figure 9

The distribution of LMC PNe (filled diamonds) and GBPNe (open squares) in the NIR colour plane. The large, dashed diamond-shaped region indicates the region of reddened GDPNe, whilst the rectangle corresponds to the regime of de-reddened GDPNe (see Ramos-Larios

& Phillips 2005). The locus for main-sequence stellar colours is taken from Tokunaga (2000). It should be noted that sources to the left-hand side of the plane correspond to nebulae in which emission is dominated by central star continua, and that the disparity between the positions of the bulge and LMC sources indicates a difference in extinction of $\Delta A_V \sim 6$ mag.



[3.6]-[8.0]

FIGURE 1

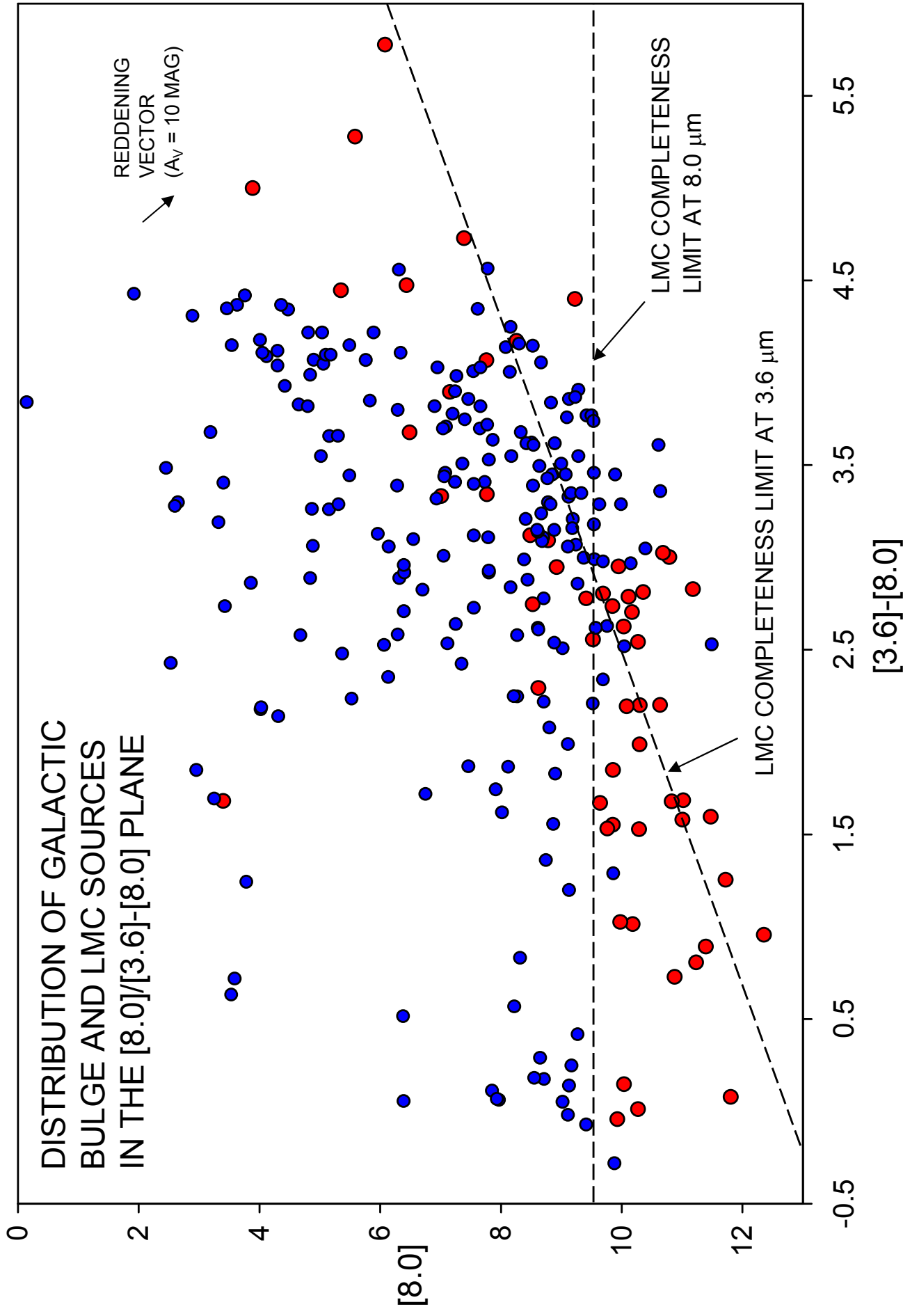


FIGURE 2

VARIATION OF BULGE AND
LMC SOURCE FRACTIONS
WITH MIR MAGNITUDES

SOURCE FRACTION

1
0.8
0.6
0.4
0.2
0

15.5 13.5 11.5 9.5 7.5 5.5 3.5 1.5 -0.5

LMC (8 μm)

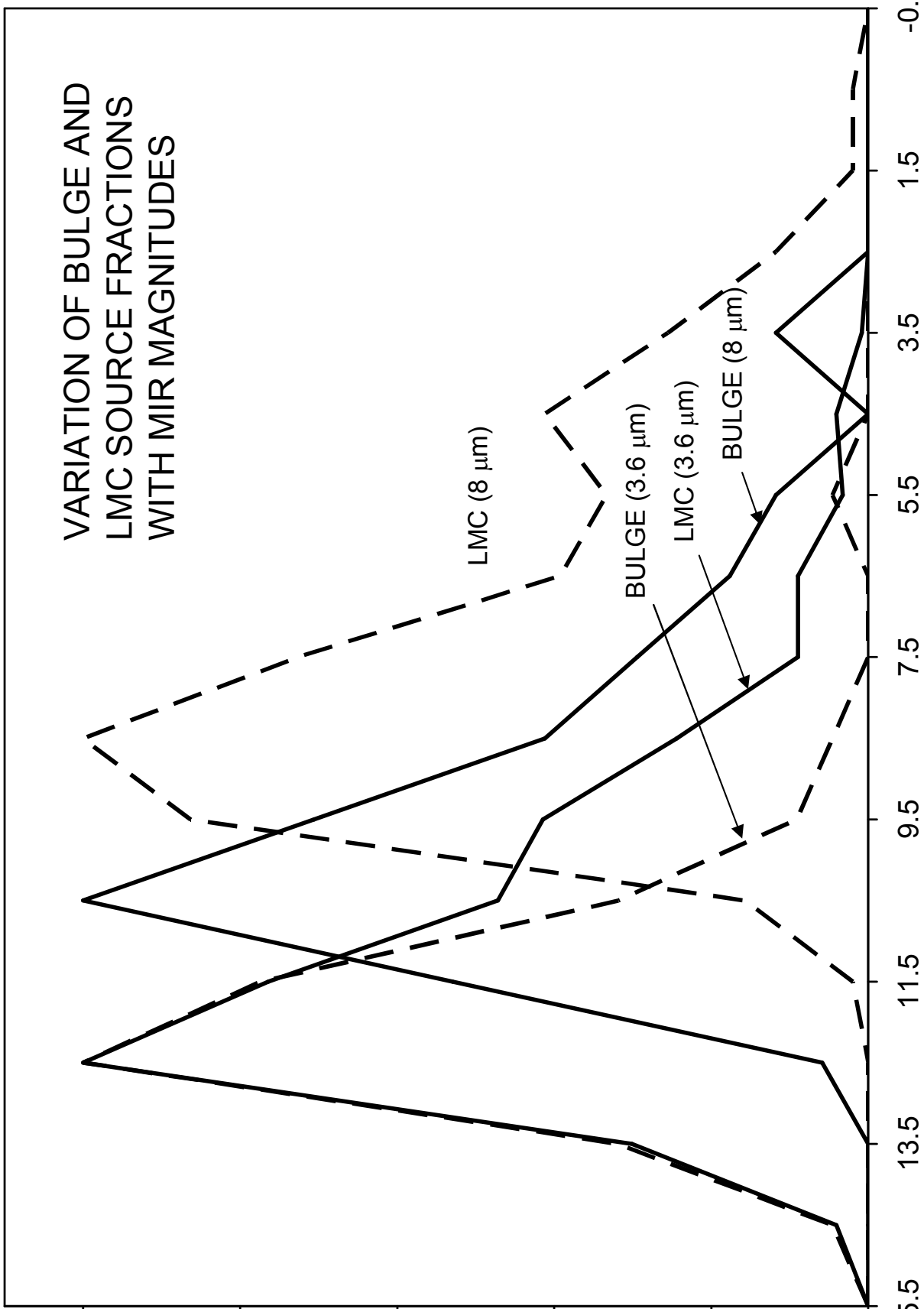
BULGE (3.6 μm)

LMC (3.6 μm)

BULGE (8 μm)

$[3.6]/[8.0]$ (mag)

FIGURE 3



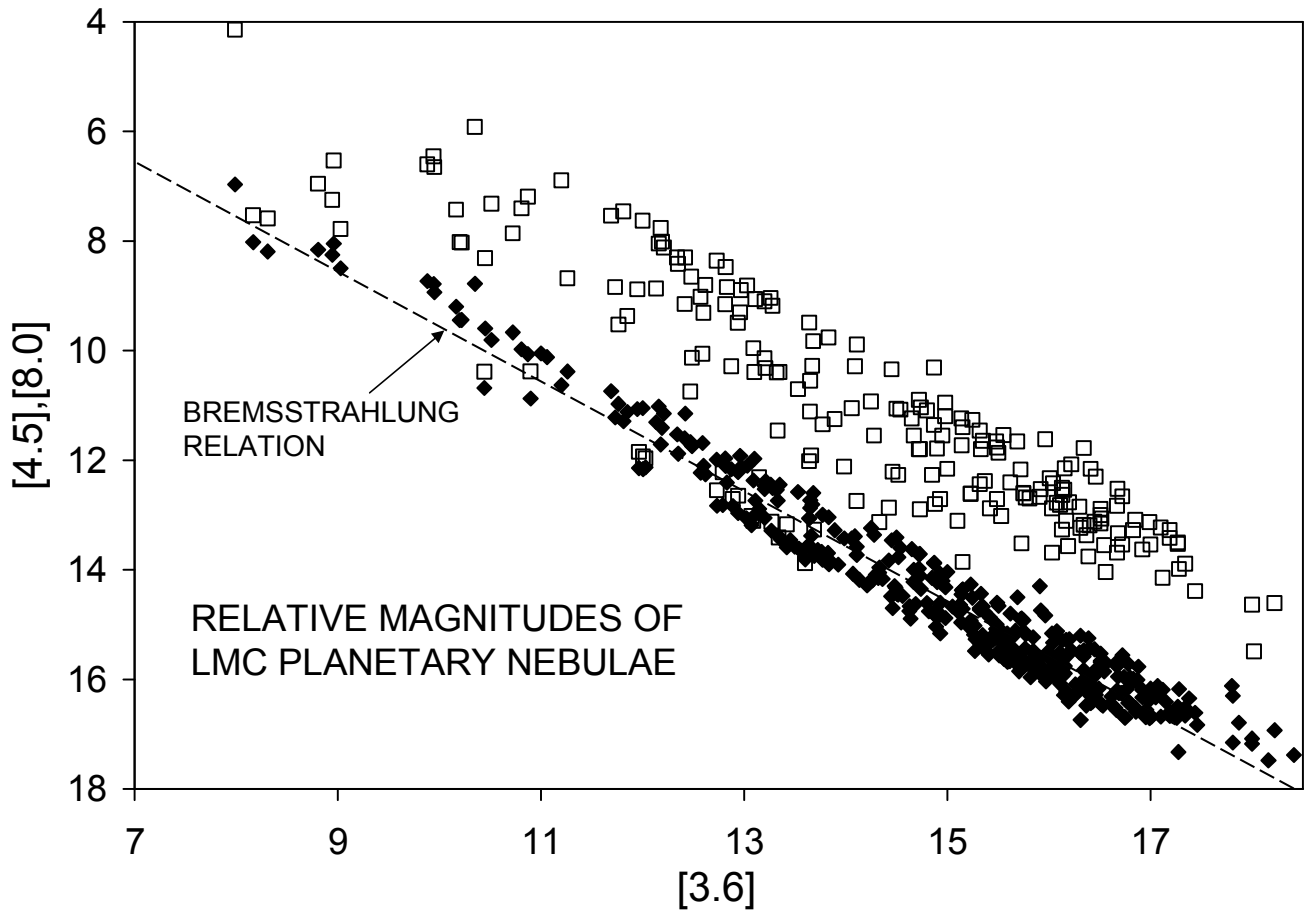
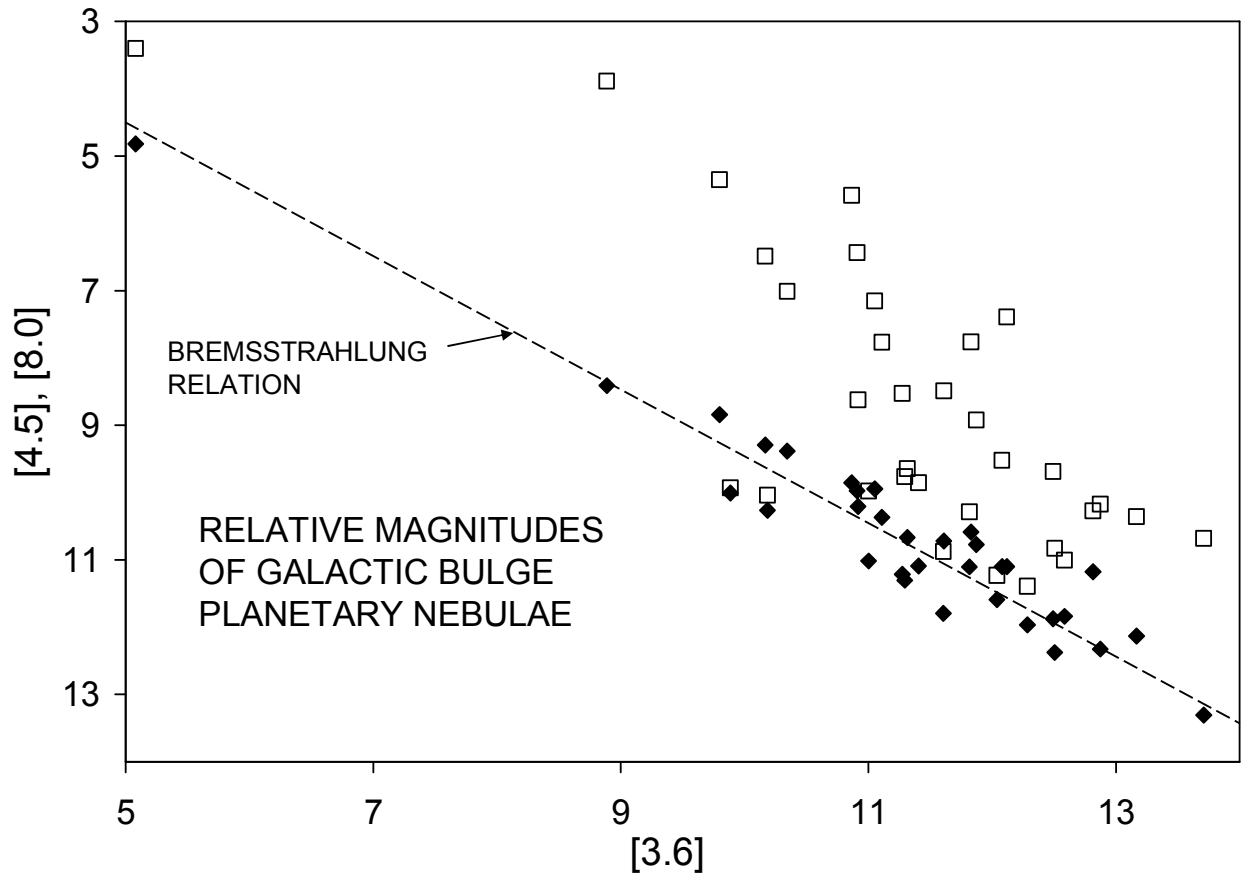
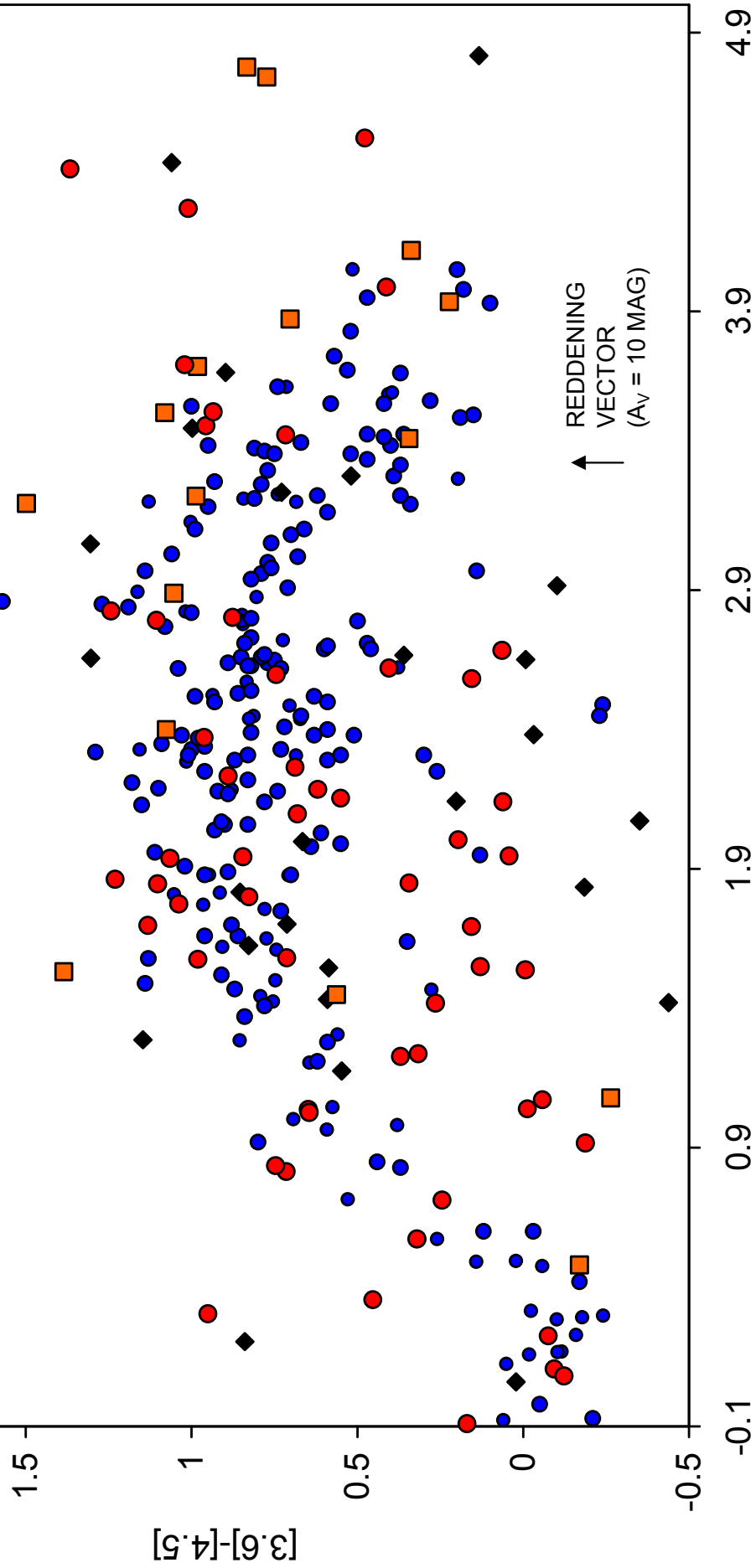


FIGURE 4

DISTRIBUTION OF GALACTIC DISK, BULGE,
AND LMC PLANETARY NEBULAE WITHIN
THE [3.6]-[4.5]/[4.5]-[8.0] COLOUR PLANE



[4.5]-[8.0]

FIGURE 5

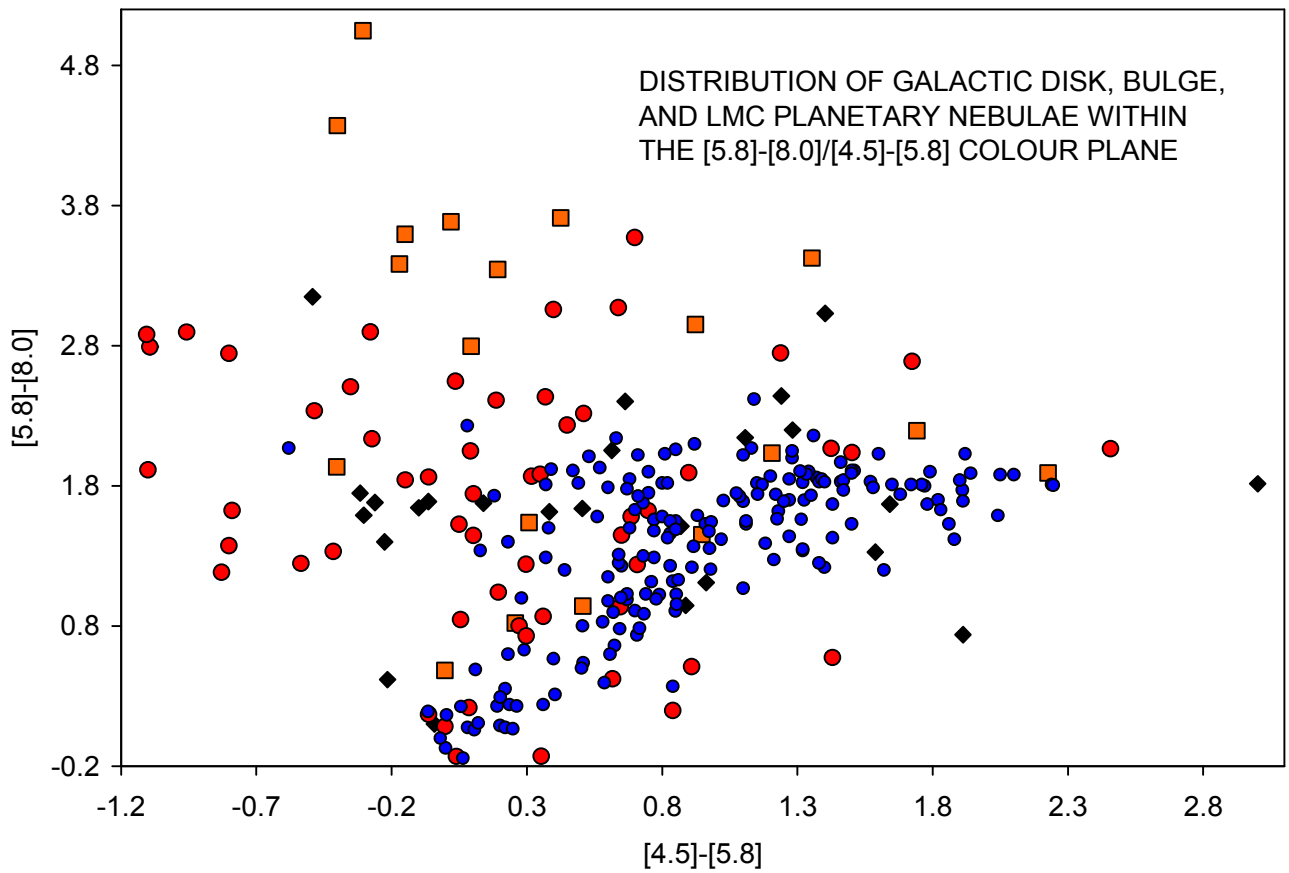
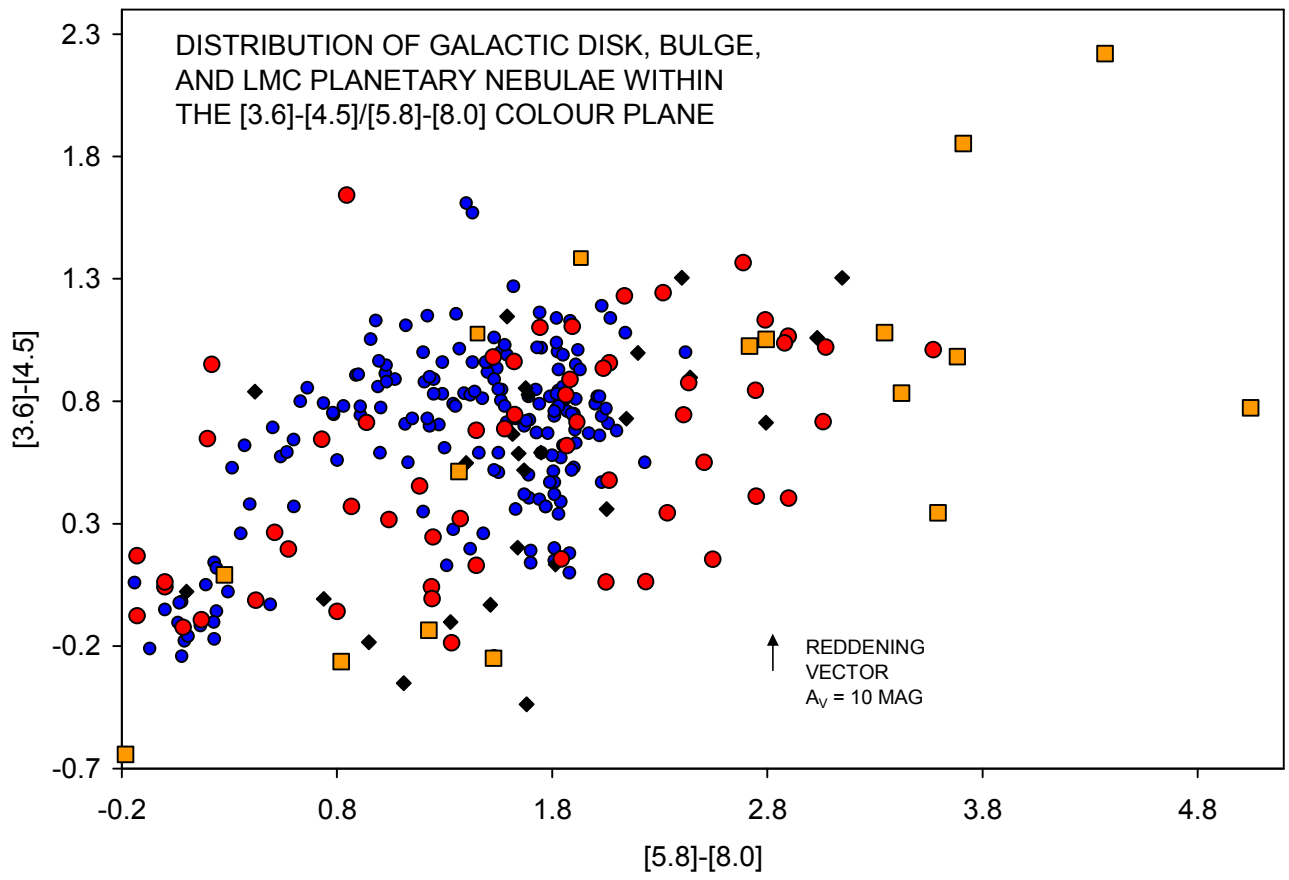


FIGURE 6

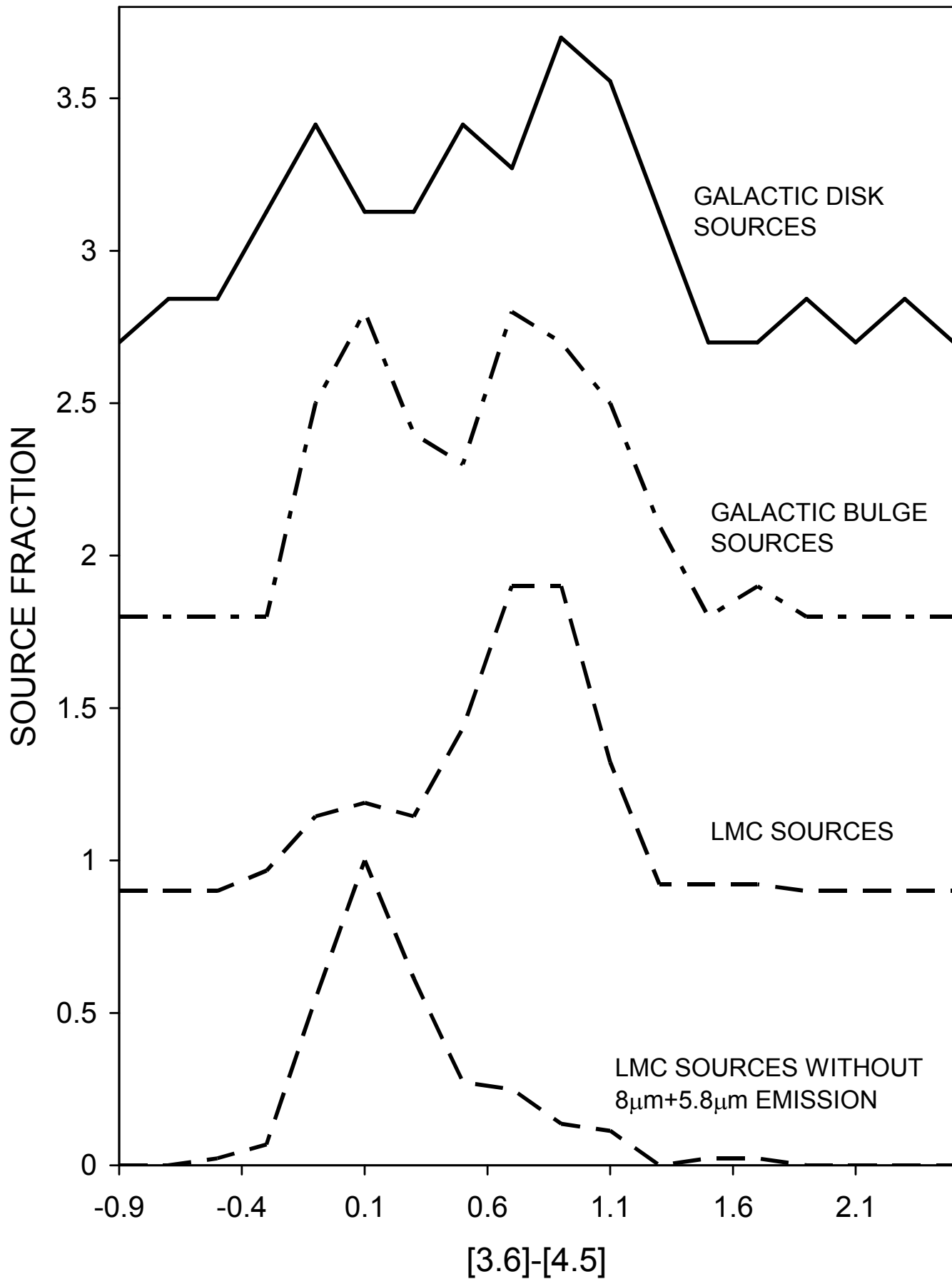


FIGURE 7

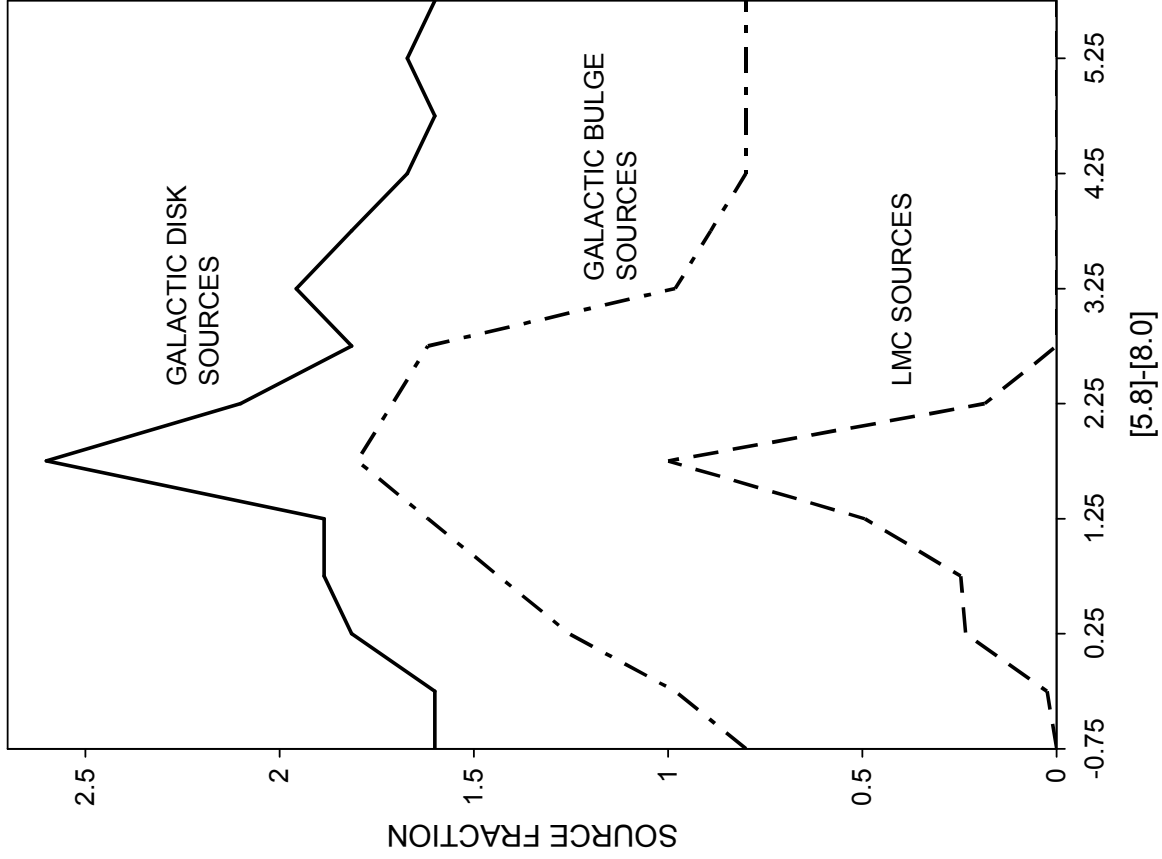
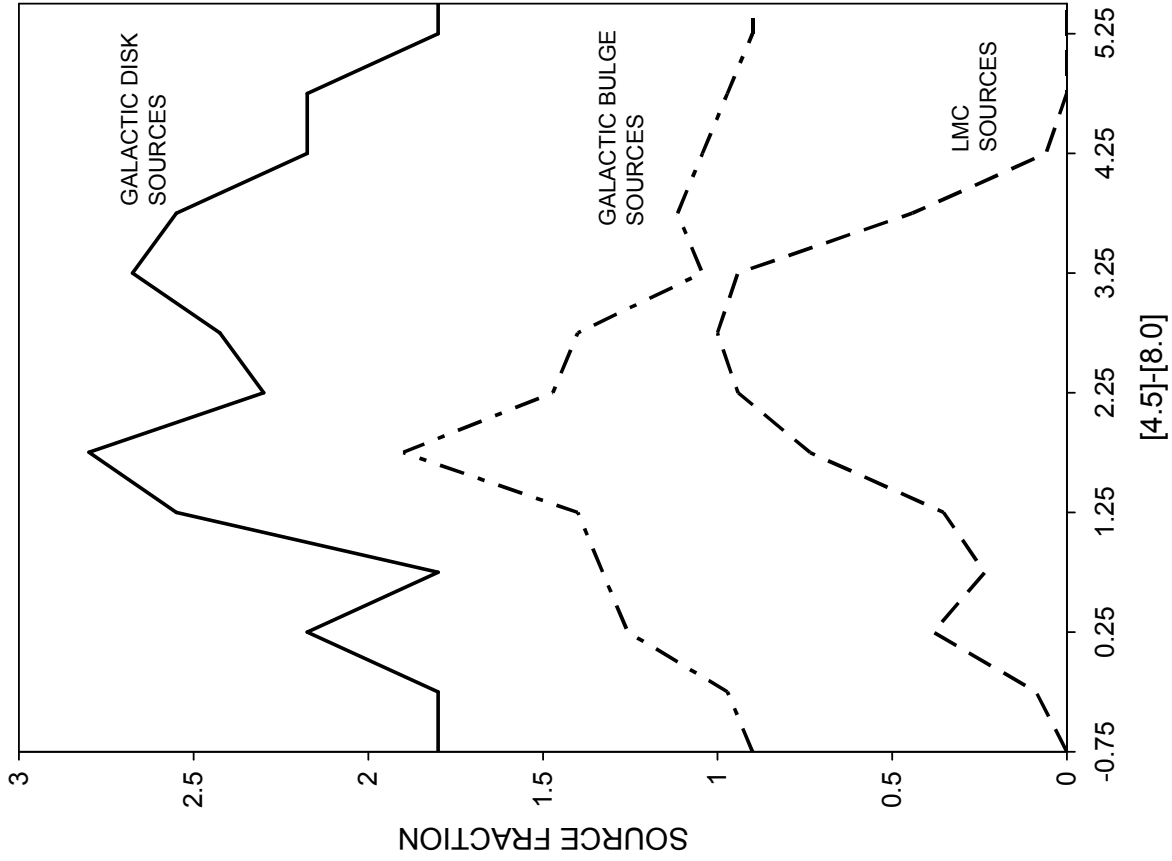


FIGURE 8

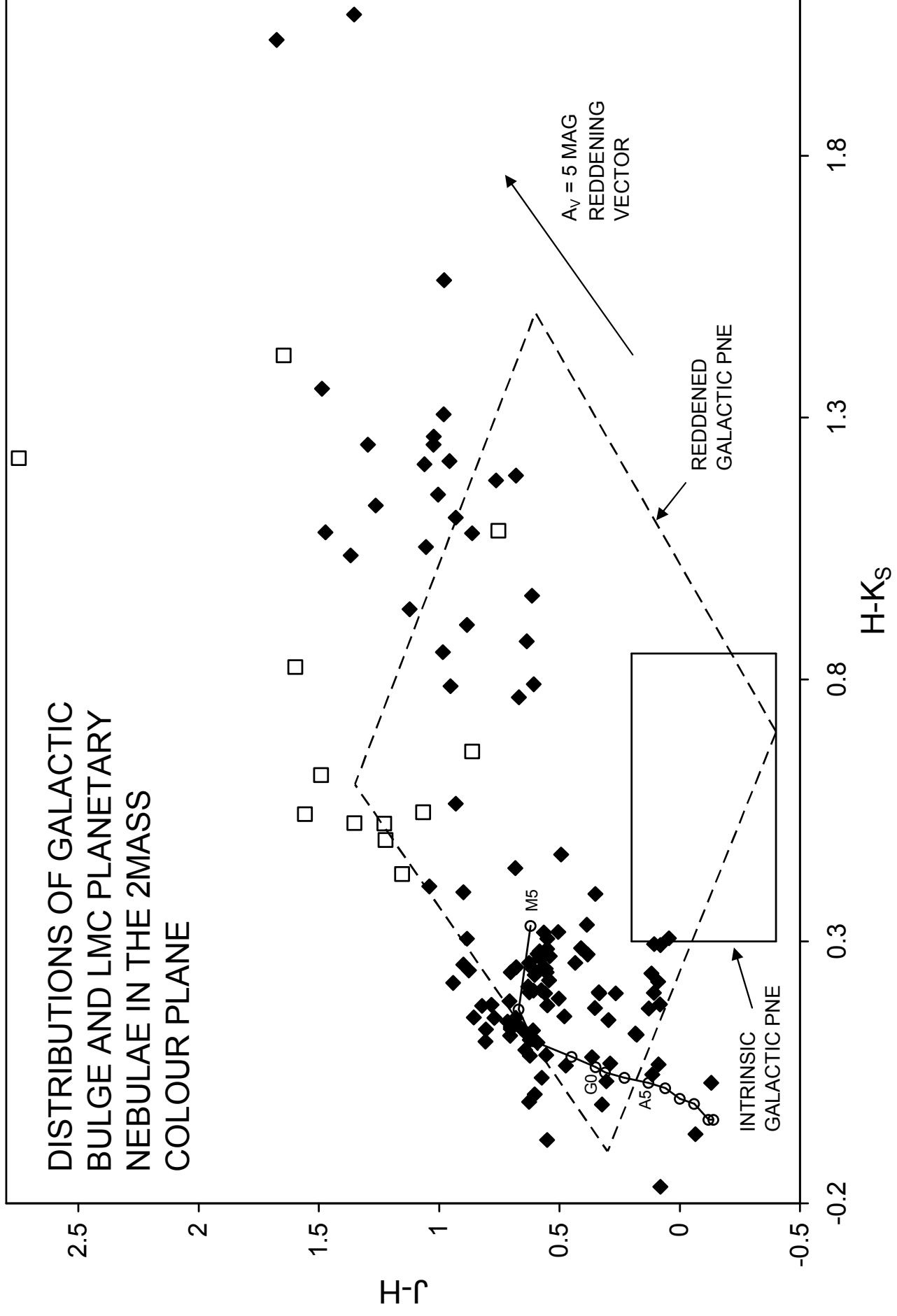


FIGURE 9